High Frequency Transformer Modelling

Transformer Subgroup

EE3L11: BAP

Stijn Verhoeven, Eliott Schuurman, Albert van der Veen

Delft University of Technology

TU Delft

High Frequency Transformer Modelling

Transformer Subgroup

by

Stijn Verhoeven, Eliott Schuurman, Albert van der Veen

Supervisor:	Dr. Mohamad Ghaffarian Niasar
Thesis committee members:	Dr. Sebastian Feld, Dr. Ir. Nick van der Meijs, Dr. Mohamad Ghaffarian Niasar
Project Duration:	April, 2025 - June, 2025
Faculty:	Faculty of Electrical Engineering, Mathematics and Computer science - TU Delft

TU Delft

Abstract

Transformers are widely used in power electronics but their low operating frequency typically makes them bulky. Increasing the switching frequency can significantly reduce transformer size, weight, and production costs, which is particularly advantageous for portable applications such as chargers. This report investigates the operation of high-frequency transformers and presents the design and development of a working prototype operating at up to 3MHz.

Electrical parameters, including inductance, capacitance, and resistance, were measured using a Bode 100 vector network analyser (VNA) and validated through analytical models and finite element simulations in COMSOL Multiphysics. Based on these parameters, a transformer model was constructed using IEEE Std 390 [1] and verified in LTSpice against measured results. Toroidal cores made of soft ferrite materials in various sizes were evaluated, and round copper wire was initially used for windings. To minimize AC resistance at high frequencies, litz wire was selected for the final prototype. The completed transformer was integrated into a switching circuit operating at 1.5MHz, demonstrating successful high-frequency performance and practical viability.

Acknowledgements

With special thanks to

Dr. Mohamad Ghaffarian Niasar for supervising the project, providing assistance as well as insight on what to research, agreeing to be on the jury and for providing valuable feedback in all stages of the project; **Dr. Ir. Hani Vahedi** for providing constructive criticism as well as being available for any uncertainties; **Dr. Ir. Wenli Shi** for providing very helpful and insightful criticism during the green light assessment; **Dr. Ir. Nick van der Meijs** and **Dr. Sebastian Feld** for agreeing to be on the jury and evaluating the project; **Luis Castro Heredia** for providing assistance in the ESP lab and helping with all equipment available in the lab; **Wim Termorshuizen** for helping in the lab; **Rik Banerjee** for assisting with any uncertainties; **Reza Mirzadarani** for providing knowledge required for proper operating and measurement using the Bode 100 VNA; **Farzad** for helping with the VNA; **Dr. Ing. Ioan E. Lager** for laying a strong foundation in the theory of EM and also being the supervisor for this entire BAP project; and **Dr. Jianning Dong** for providing a strong foundation in the theory of electrical machines and in particular the workings of a transformer.

Contents

1 Introduction

1.1. State-of-the-Art Analysis

High-frequency transformers (HFT) are a type of transformer that operates at frequencies higher than the standard net frequency of 50/60 Hz. These frequencies range from tens of kilohertz up to several megahertz. In power-dense, high-efficiency systems such as EV chargers [2] and renewable energy converters [3], HFT play a critical role in the development of smaller and lighter designs. Other applications for the high-frequency transformer include, but are not limited to: switch-mode power supplies [4], arc welding [5], medical imaging equipment [6], and induction heating [7]. By operating in the high-frequency range, these transformers reduce magnetic component size, allow for increased power density and offer better integration with fast-switching semiconductors. However, such benefits come with a set of complex technical challenges.

1.1.1. Dominant Challenges

The transformer core experiences losses, called core losses, in the form of hysteresis and eddy currents [8]. Due to non-linear dependency, at high frequencies the losses become significant. Winding losses due to the skin and proximity effect reduce the effective conduction area, significantly raising the AC resistance. These effects are particularly pronounced in toroidal windings, where the conductor arrangement is more constrained than in other geometries. Litz wire and foil windings are capable of reducing the winding losses. A third factor is the distributed capacitance between windings (inter-winding), between winding turns (intra-winding) and between the winding and the core. Also called stray capacitance or parasitic capacitance, it acts like a shunt capacitance, conducting high-frequency currents [9]. In high-frequency operation, this introduces resonances, overshoots and common mode noise [10]. Additionally, these parasitics can also distort switching behaviour in power stages, especially when fast GaN or SiC switches are used [11].

1.1.2. Existing Modelling Techniques

In response to these challenges, three main modelling strategies have emerged:

- **Analytical** models are fast and intuitive, though typically rely on simplified assumptions: linear material behaviour, uniform flux distribution and/or neglect of higher-order effects such as frequency dependent winding resistances. For example, for core loss calculationsmodified Steinmetz equations (iGSE) are used.
- **Numerical** methods, particularly Finite Element Modelling (FEM) provide high fidelity electromagnetic field simulations. Tools like COMSOL and ANSYS Maxwell can model field distributions, parasitics and thermal profiles, but are computationally intensive and introduce their own complications (e.g. mesh convergence issues).
- **Empirical** characterisation, through means of measuring real components and extracting equivalent circuit parameters. One such method for extraction is the IEEE Std 390 [12].

1.1.3. Gaps in Literature

The IEEE 390 outlines procedures for extracting transformer equivalent circuits based on frequency dependent impedance measurements. Values extracted are the equivalent resistances, reactances and parasitic capacitances. While the method is established for conventional frequencies, it has not been evaluated for MHz-range designs. Related works use methods such as the reflection coefficient technique with the scattering matrix [13] and the more commonly seen frequency response analysis (FRA) [14], [15] to extract circuit parameters, however these do not explicitly reference the IEEE 390. Even fewer papers explore the differences between analytical, numerical and empirical derivations of parameters, presenting both a risk and an opportunity. The design and validation of a HFT using IEEE 390, supported by real builds, equivalent circuit modelling, and FEM simulation, therefore represents a valuable contribution to research.

1.2. Problem Definition

1.2.1. Situation Assessment

Historically, transformer modelling was based on lumped parameter approaches suited for low frequency operation, where parasitic capacitances and frequency-dependent losses were negligible [8], [16]. As switching frequencies have increased into the MHz range, these assumptions no longer hold. Modern systems such as EV chargers and power-dense converters demand models that account for skin effect, proximity losses, thermal behaviour, and electromagnetic interference [17], [18]. While FEM tools and empirical methods exist, they are often computationally intensive or lack standardisation. Currently, no widely accepted workflow integrates analytical, numerical, and measurement-based methods for MHz-range toroidal transformers. This project addresses that gap by evaluating whether equivalent circuit parameters extracted via IEEE 390 can form the basis of a reliable modelling and validation framework at high frequencies.

1.2.2. Scoping Analysis

Needs

The Dutch energy transition demands a fundamental rethinking of how we handle energy conversion and distribution. In a power landscape populated by decentralised renewable sources, compact and efficient conversion hardware is crucial. Traditional low frequency transformers cannot support the required power density or control dynamics. In addition to this, nearly 35% of new car registrations in the Netherlands are battery electric vehicles (BEV) [19], and the electric fleet is expected to grow further. HFT are critical components in onboard EV chargers, supporting the energy transition at both household and grid levels. In this context, HFT are not just relevant - they're essential. Despite their growing importance, accessible and standardised modelling methods for high-frequency transformers are lacking.

Objectives

This project aims to develop and validate a design workflow that incorporates the IEEE 390 equivalent circuit models for high-frequency transformers. The goal is to assess whether these models, calibrated with experimental results and benchmarked against analytical calculations, can form a reliable, practical design. If successful, this workflow would reduce the reliance on trial-and-error or costly simulation loops and provide transformer designers (especially in automotive and power systems industries) with a systematic and efficient design and evaluation tool.

SMART Criteria

- **Specific**: Implement and verify the IEEE 390 model for at least three HFT prototypes operating between 1–3 MHz.
- **Measurable**: Achieve a maximum deviation of 10% between simulated and measured values across the bandwidth of interest.
- **Assignable**: All tasks related to design, modelling, and measurement are carried out by the thesis subgroup in a divided, efficient and documented manner.
- **Realistic**: The target accuracy is aligned with what's achievable in practical HFT modelling without resorting to full 3D FEM tools such as COMSOL.

- **Time-related**: The modelling, testing, and validation for all transformer prototypes must be completed within the 8 week thesis timeline.

1.2.3. Bounding Analysis

In order to implement, verify and create a working HFT prototype, certain constraints, parameters and variables need to be defined. These highlight the limitations of the project.

Constraints

The constraints follow from the needs of the project.

- The transformer must operate within 1-3 MHz, based on the requirements for compact power converters in electric vehicles.
- Thermally, the transformer must operate safely under passive or forced air-cooling, as is done in automotive or residential applications.
- Commercially available cores and copper wire may be used, reflecting realistic production feasibility.
- Total material cost per prototype may not exceed €200, aligning with small scale industrial products (and the BAP framework), assuming power handling requirements for portable applications.
- All modelling, testing and validation must be completed within the EE3L11 8-week window.

Parameters

Factors that affect ability to make alternatives are called parameters or alterables. These are as follows:

- Winding configuration: number of turns, wire gauge, spacing, layering strategy.
- Core selection within commercial availability in mind. Different shapes, sizes, materials.
- Frequency range between 1-3 MHz to assess performance.
- Measurement setup consistency. Are test voltages the same? Are followed procedures consistent?

Variables

The transformer will be modelled, tested and validated against different methods, whether these be analytical, numerical or empirical. What variables are measured for monitoring the performance?

- Leakage and magnetising inductance
- Equivalent resistance and core loss values
- Parasitic capacitances
- Temperature under nominal load conditions
- Transformer efficiency
- Deviation between analytical models and simulations

1.3. Thesis Synopsis

This thesis investigates the design, modelling, and performance evaluation of high-frequency transformers for MHz-range applications. Multiple prototypes are constructed and characterised using the IEEE Std 390 procedure to extract equivalent circuit parameters. These are compared against analytical predictions and FEM simulations to assess model accuracy. A final prototype is built based off of the values required by the switching circuit subgroup. The aim is to evaluate whether IEEE 390 provides a practical and reliable modelling framework for high-frequency transformer design.

2

Programme of Requirements

The overall aim of the project is to make a working DC-DC converter, as shown in figure 2.1. It consists of a switching circuit, generating a high-frequency AC signal; a transformer capable of handling the high frequency and wirelessly transforming the signal to the secondary side; and a rectifier to convert the AC signal back into DC. This thesis discusses the highlighted transformer component.

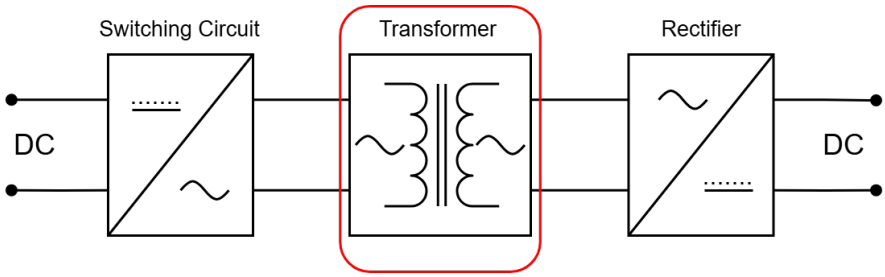

Figure 2.1: Total schematic for a DC-DC converter.

The aim for the transformer subgroup is to design, model, and evaluate a high-frequency transformer in the megahertz range for power conversion applications, such as EV chargers, renewable energy systems and compact electronics. Focus is placed on optimising core materials, winding configurations, and thermal management to minimise winding/core losses and maximise efficiency. Use of simulation tools like COMSOL or MATLAB for validation, after which experimental testing is conducted to measure performance (efficiency, thermal behaviour, losses). Results are compared with theoretical models, discrepancies analysed, and design improvements proposed. A professional grade transformer prototype is delivered with documented performance metrics.

A set of requirements has been outlined below. One set is related to the transformer itself, and the second set to the testing and measurement of the transformer.

2.1. Transformer Product

No.	Requirement	Type	Test
1	The transformer must convert an AC signal generated by a switching circuit as part of a DC–DC power conversion system.	Functional	Observe AC–AC transformation and DC output post-rectification.
2	The transformer must operate at 2 A, 50 V, delivering 100 W.	Functional	Measure current and voltage under nominal load.
3	The transformer must be bidirectional (does not matter what the primary or secondary side is) with a 1:1 turns ratio.	Construction	Visual inspection and functional verification.
4	The transformer must have two input and two output terminals.	Construction	Physical inspection of winding terminations.
5	The transformer must maintain $\geq 80\%$ efficiency at full load.	Performance	Compare input and output power at 100 W.
6	The transformer must operate at ≥ 1 MHz without core saturation.	Performance	Measure waveform distortion and compare to B_{max} estimates.
7	The transformer core temperature must remain below its Curie temperature, and winding insulation must remain within rated limits.	Boundary	IR thermometer or thermocouple measurement under steady-state operation.
8	The transformer must be cooled using passive or forced air (80 mm fan).	Boundary	Observation of cooling setup during tests.
9	The complete transformer and driving circuit must fit within an $8 \times 8 \times 5$ cm enclosure.	Boundary	Physical measurement of prototype dimensions.

Table 2.1: Programme of Requirements for Transformer Product

2.2. Testing and Measurement

No.	Requirement	Type	Test
1	Impedance measurements across the 1-3 MHz range must be taken using an LCR meter or network analyser.	Functional	Perform impedance sweep with test equipment.
2	Equivalent circuit parameters must be extracted using IEEE Std 390.	Functional	Document procedure and parameter values.
3	The core and winding losses must be estimated analytically, simulated, and measured experimentally.	Performance	Cross-compare losses from all three methods.
4	The temperature rise must be measurable using thermocouples or an IR camera.	Functional	Set up and validate measurement rig.
5	Efficiency at 100 W must be calculated based on input-output power measurements.	Performance	Use oscilloscope and power probes.
6	The transformer must support repeatable testing under fixed load conditions.	Boundary	Implement standardised test load setup.
7	The transformer model must be simulated using COMSOL Multiphysics to validate extracted parameters and support analytical comparison.	Functional	Run simulations in COMSOL using measured geometry and materials; compare outputs to IEEE 390 and analytical results.

Table 2.2: Programme of Requirements for Testing and Measurement

3

Theory

3.1. Physics

3.1.1. Ampère's Law

Ampère's Law relates the circulation of a magnetic field around a closed loop to the current that passes through said loop. It is fundamental in transformers because it relates the magnetomotive force from coil currents to the magnetic field in the core, enabling the calculation of flux. The flux, in turn, determines the induced voltages in the windings via Faraday's Law (explained in 3.1.2). The integral form is given below.

$$\oint_C \vec{H} \cdot d\vec{l} = \iint_S \vec{J}_{free} \cdot d\vec{S} = I_{free,enc} \tag{3.1}$$

Equation 3.1 is Ampère's Law using $\vec{H}$, magnetic field intensity. It is related to the magnetic field density through the constitutive relation $\vec{B} = \mu_0 \vec{H}$.

3.1.2. Faraday's Law

Faraday's Law of induction predicts how a magnetic field will interact with an electric circuit to produce an electromotive force (emf). It is crucial in transformers because it describes how a time varying magnetic flux induces voltage in the windings. This induced voltage enables energy transfer between the primary and secondary circuits without electrical contact. Equation 3.2 states that the emf ε is given by the rate of change of the magnetic flux Φ_B scaling with the number of turns.

$$\varepsilon = -N\frac{d\Phi_B}{dt} \tag{3.2}$$

Equation 3.2 is for a tightly wound coil of wire, where N is the number of identical turns and Φ_B the magnetic flux through a *single* loop.

3.1.3. EMF equation

Core saturation is a phenomenon where the magnetic materials B-H curve is in the non-linear region. This implies that with an increase in the magnetizing force (H), the flux density (B) does not necessarily increase linearly, as the permeability (μ) of the material decreases. This will produce a non sinusoidal waveform and result in magnetic losses. To find the conditions at which the core saturates, Equation 3.3 can be used.

$$\varepsilon = \frac{2\pi}{\sqrt{2}} f N B_{max} A_c \tag{3.3}$$

This equation follows from a combination of Ampère's law and Faraday's law for solenoids where the number of turns plays a role in both cases. The assumption is made that the current through the Amperian loop is a pure sinusoidal with intensity I, giving the current as $I(t) = I\sin(\omega t)$. The magnetic field density can be found by applying Ampère's law to the sinusoidal current:

$$\oint B \cdot dl = \mu N I \sin(\omega t) \tag{3.4}$$

Working this out will give $B(t) = \frac{\mu N I \sin(\omega t)}{l}$. Now to find the flux through a surface which is used for Faraday's law, a surface integral of the magnetic flux density has to be done:

$$\phi(t) = \oint B(t) \cdot dS \Rightarrow \phi(t) = \oint \frac{\mu N I \sin(\omega t)}{l} \cdot dS \tag{3.5}$$

Once the flux is known, Faraday's law (for solenoids) is applied. One thing to note is that all the derivations are done using a sinusoidal current signal. However, it is much more interesting to look at the RMS values of the signal, since it eliminates the time varying part. This will make further calculation easier:

$$\varepsilon_{rms} = -N\frac{d\phi}{dt} \Rightarrow \varepsilon_{rms} = -\frac{\mu A N^2 I \omega}{l}\cos(\omega t) \Rightarrow \varepsilon_{rms} = \frac{\mu A N^2 I 2\pi f}{l\sqrt{2}} = \frac{2\pi}{\sqrt{2}} f N B A_c \tag{3.6}$$

Since the transformer core will saturate at B_{max}, we know that we cannot apply a voltage larger than a certain value. The RMS value for a sine wave is calculated by simply dividing the intensity by $\sqrt{2}$. This follows from the definition of the RMS: $RMS = \sqrt{\frac{1}{T}\int_t^{t+T}(x(t))^2 dx}$. This is proven here:

$$\cos(\omega t) = -\sin(\omega t - \frac{\pi}{2}) \Rightarrow \sqrt{\frac{1}{2\pi}\int_0^{2\pi}(-\sin(\omega t - \frac{\pi}{2}))^2 dx} = \frac{1}{\sqrt{2}} \tag{3.7}$$

3.1.4. Inductance

Self Inductance

The self inductance of a primary winding in a non-ideal transformer can be expressed analytically as:

$$L_1 = \frac{\mu_r \mu_o A_c N_1^2}{l_c} = \frac{N_1^2}{\mathcal{R}} \tag{3.8}$$

Where L_1 is the self inductance of the primary winding, μ_r is the relative permeability of the core material, μ_0 is the absolute permeability of free space, A_c is the effective cross-sectional area through which the magnetic flux links the winding, N_1 is the number of turns on the primary side, and l_c is the mean magnetic path length of the core. The values μ_r, A_c and l_c are found in the datasheets of the respective core material. The core reluctance $\mathcal{R}$ is a constant, representative of the opposition to magnetic flux and analogous to electrical resistance. It is defined as:

$$\mathcal{R} = \frac{l_c}{\mu_r \mu_0 A_c} \tag{3.9}$$

Expression (3.8) is derived from the definition of inductance, $L = \lambda/i$, where $\lambda = N_1\phi$ is the magnetic flux linkage. Applying Ampère's Law and assuming linear magnetic behaviour, the flux ϕ generated by the current in the winding is related to the magnetomotive force and core reluctance by:

$$\phi = \frac{N_1 i}{\mathcal{R}} = \frac{N_1 i \mu_r \mu_0 A_c}{l_c} \tag{3.10}$$

Substituting into the flux linkage expression and rearranging yields the inductance formula (3.8) above.

Coupling Coefficient k

Not all the magnetic flux produced by the primary winding is coupled to the secondary side. Some of the magnetic flux "leaks", and is therefore called leakage inductance. The mutual flux is given below:

$$M = k\sqrt{L_1 L_2} \tag{3.11}$$

Where k is the coupling coefficient. It is a measure of how close the magnetic fields of two inductors are interlinked, and has values $0 \leq k \leq 1$. When k = 1, the two windings are perfectly coupled and no leakage of the magnetic flux is present. Equation 3.11 can be rewritten to be:

$$k = \frac{M}{\sqrt{L_1 L_2}} \tag{3.12}$$

Which is *a* method of calculating k. The magnetising and leakage inductance can be calculated from knowing k and the self inductance of the coil. Formulas are:

$$L_{mag} = kL \tag{3.13}$$

$$L_l = (1 - k)L \tag{3.14}$$

Magnetising and Leakage Inductance

The magnetising and leakage inductances stem from the self inductance of the coil L. It is the same for the primary side as it is for the secondary side, so:

$$L = L_{mag} + L_l \tag{3.15}$$

The magnetising inductance L_{mag} represents the portion of a transformer's self inductance associated with magnetic flux that links both windings (mutual flux) under perfect coupling (so k = 1). It is finite when the core has a finite permeability, and it determines how much current is needed to establish magnetic flux in the core when the secondary side is open-circuited [9]. On the other hand, the leakage inductance L_l represents the portion of a transformer's self inductance due to magnetic flux that does *not* link both windings. This can be flux in air gaps, insulation, or fringing paths. Energy is stored locally around each winding and is modelled as a series inductance, reducing the coupling efficiency (k < 1) and affecting high-frequency performance. At high frequencies, the leakage inductance contributes to:

- Voltage drops
- Waveform distortion and ringing due to resonance with parasitic capacitances
- Reduced efficiency and bandwidth in fast switching circuits

To reduce the leakage inductance, windings can be placed over one-another and the number of turns should be reduced [9].

3.2. Core Saturation

When applying an external magnetic field to a ferro-magnetic core, it will magnetise. The relation between magnetic flux density and magnetic field intensity is given by H = μB [20]. However, at a certain point the linear relation between the intensity and density will stop. This is clearly illustrated in a B-H curve, for example figure 3.1. This phenomena is explained by the fact that the magnetic core consists outs of many small ferro magnetic regions. These regions will turn in the same direction when exposed to an external magnetic field. At some point all these regions will be aligned, leaving no room for further alignment [21]. For an increase in current, which results in an increase of H due to Ampère's law, the magnetic field density will increase - but only by a small amount.

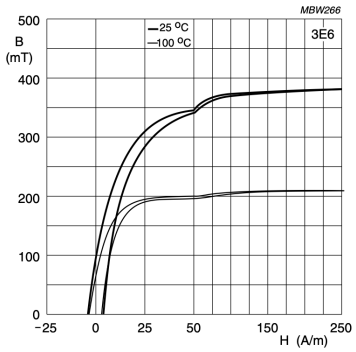

Figure 3.1: B-H curve of the medium toroid [22].

The non-linear magnetic field density increase will result in a non-perfect voltage curve. Once more, this can be explained by Faraday's law. From equations 3.4 and 3.5, it can be seen that ε is given by $\varepsilon = -NIA\frac{dB}{dt}$. Looking back at the corresponding B-H curve, it can be seen that for a linearly increasing H, B will at some point not increase linearly but instead plateau. Meaning that the derivative of the magnetic field density will tend towards 0 for a small period of time. Since ε is linearly dependent on that derivative, it too will be 0 for a small period of time. This will create a sort of "dead-time" around the x-axis.

3.3. The Transformer

3.3.1. Core Type

The shape and size of a core can influence the electromagnetic performance, efficiency, cost and ease of manufacturing. Several core types are commonly used, each having their advantages and limitations, such as:

- **Toroidal Cores**: Consist of a continuous, closed and circular magnetic path, which results in the majority of magnetic flux staying within the core material. This results in low leakage inductance and minimal EMI. Kazimierczuk, [9], highlights that toroidal cores have the lowest EMI emissions and offer excellent heat removal. Therefore, toroids are a good fit for high frequency applications. Winding is labour intensive, but the pay-off is good EMI performance.

Figure 3.2: Toroidal core [23].

- **Pot Cores**: These cores *almost* surround the entire winding, resulting in good protection from EMI. However, pot cores are generally more expensive and are less effective at heat dissipation.

Figure 3.3: Pot core [24].

- **Double Slab and RM Cores**: Modified pot cores that have sections cut off, allowing for better heat dissipation and larger wires. RM cores reduce the used board space and are thus suitable for compact printed circuit board (PCB) applications.

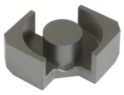

Figure 3.4: RM core [25].

- **E Cores**: Feature open windings, allowing for simple winding configuration and assembly, but at the cost of increasing EMI. They allow for good airflow and are typically less expensive. There are different sizes and can be placed in different orientations, resulting in various usable cases.

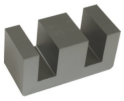

Figure 3.5: E core [26].

- **EC, ETD and EER Cores**: A mix of E cores and pot cores. Like E cores, they provide wider winding windows, allowing for larger wires and better heat dissipation due to increased airflow. The round centre limits sharp bends in the wires, reducing losses.

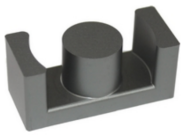

(a) EER core & ETD core [27].

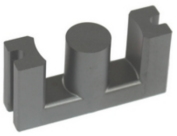

(b) EC core [28].

Figure 3.6: EC, ETD & EER cores

- **PQ cores**: Optimised for switched-mode power supplies, resulting in maximum inductance and winding area with minimum core sizes. The high winding area-to-volume ratio allows for bigger wires and better thermal management.

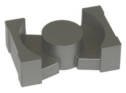

Figure 3.7: PQ core [29].

- **EP cores**: Almost entirely enclosed, except for the PCB terminals. This design provides very good EMI protection and minimizes air gaps, ensuring good magnetic performance. Thermal dissipation is limited due to the enclosed windings.

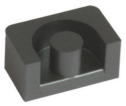

Figure 3.8: EP core [30].

3.3.2. Core material

To operate at high frequencies without losses, determining what core material to use is essential for a successful HFT. The major parameters of a HFT core material should be as follows:

- **High saturation flux density** B_s: Larger B_s translates to more energy transfer per cycle or reductions in the core cross-section for a given power, therefore directly boosting power density.

- **High curie temperature** T_c: The core must be able to operate safely under sustained temperatures without breaking or losing its magnetic order. The Curie temperature is defined as the temperature above which a material loses its permanent magnetic properties. This differs per material.

- **Low magnetostriction** λ: Magnetostriction drives the vibration and acoustic noise as the flux varies due to an applied magnetic field. No deviation in the volume of the core is desired, and the magnetostriction should therefore be low.

- **High relative permeability** μ_r: A high μ_r lowers the magnetizing current for a given inductance, improving coupling and reducing reactive losses.

- **Low coercivity** H_c: H_c is the coercivity and represents the ability of a magnetic material to withstand demagnetization. It determines the area of the hysteresis loop and thus hysteresis loss in the transformer. A low coercivity material is said to be a magnetically soft material.

- **High resistivity** ρ: A high resistivity suppresses the eddy currents in the core at high frequencies.

- **Low loss** P_{loss}: Core losses are directly linked to degradation in efficiency and increases in thermal stress.

- **Low cost**: The transformer must be feasible to make. It is worth exploring cutting-edge technology and rare materials, but that is ultimately not the aim of the thesis.

Four families of soft-magnetic materials (SMM) dominate in the HFT market [31]. These are Fe-Si alloys, soft ferrites, amorphous alloys and nanocrystalline alloys. The table below summarises the key features and lists the characteristics of the SMMs:

SMM family	Max. μ_r	H_c, A · m^{-1}	B_s, T	T_c, °C	ρ, Ω · m	Typical frequency range
Fe-Si alloys						Line frequency - few kHz
Non-oriented Fe-Si	$3 \cdot 10^3 – 10 \cdot 10^3$	30 – 80	1.96 – 2.12	725 – 765	$50 \cdot 10^{-8}$	
Grain-oriented Fe-Si	$15 \cdot 10^3 – 80 \cdot 10^3$	4 – 15	2.02	750	$45 \cdot 10^{-8}$	
Soft ferrites						Hundreds of kHz - several MHz
MnZn	$10^3 – 10^4$	5 – 20	0.4 – 0.55	130 – 280	0.1 – 20	
NiZn	$10^2 – 10^3$	20 – 200	0.2 – 0.35	110 – 400	$10^3 – 10^7$	
Amorphous alloys						Tens of kHz - low MHz
Fe- based	10^5	2 – 5	1.56	415	$120 \cdot 10^{-8} – 140 \cdot 10^{-8}$	
Co- based	$5 \cdot 10^5$	0.5 – 1	0.62	320	$120 \cdot 10^{-8} – 140 \cdot 10^{-8}$	
Nanocrystalline alloys						100 kHz - several MHz
FINEMET	$5 \cdot 10^5$	0.5 – 1	1.24	600	$118 \cdot 10^{-8}$	
NANOPERM	$5 \cdot 10^4$	3	1.52	600	$118 \cdot 10^{-8}$	

Table 3.1: SMM core characteristics, [31], [32]

For the scope of a >1 MHz transformer, the core materials that were found to be suitable are: soft ferrites [33], [34], amorphous alloys and nanocrystalline alloys [35], [36]. The core materials that were found to **not** be suitable are: Fe-Si alloys, due to their huge eddy losses above 1kHz [31]; and powder cores, due to their massive losses at high frequencies [33]. Thus far, soft ferrite materials are the most appropriate. Nanocrystalline alloys are very expensive and therefore not realistic as a core material.

3.3.3. Windings configuration

There were two winding topologies which were tested for the different core types. Configuration 1, where the windings were wound on opposite sides of the core and configuration 2, where the windings were wound on the same side but were intertwined. These 2 configurations were extensively tested and results noted down in a spreadsheet for further investigation. This way, trends may be spotted or validated regarding parasitics and leakages. This creates an intuitive feel for the designing of a prototype with specification for the switching circuit.

3.4. Transformer model

For simulation in programs such as LTSpice a (circuit) model is needed to be simulated. For this project the model for simulation taken is the IEEE Std 390 model, as shown in figure 3.9[37]. The

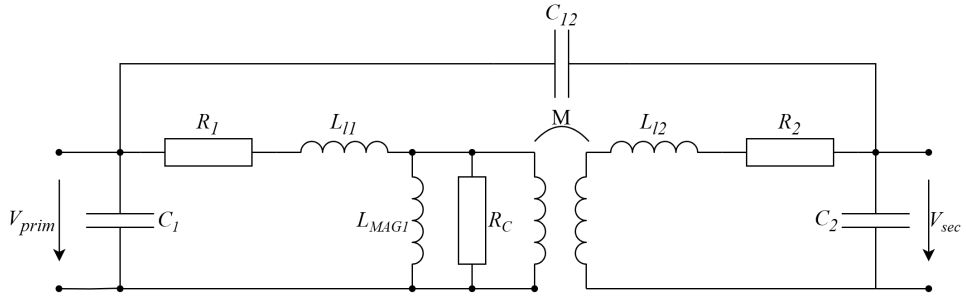

Figure 3.9: Standard transformer model for high frequencies.

main difference of this model as compared to other standard transformer models are the inclusion of (self)capacitances. These capacitances usually do not play a significant role because typical transformers do not operate at high frequencies. The impedance of a capacitor is given by $Z = \frac{1}{j\omega C}$, and since

the frequency is really low so will be the impedance. The capacitor will then act as an open circuit. This will result in the more familiar transformer model for low frequencies.

3.4.1. Capacitances

There are 2 main capacitances in this model: C_{12} & C_1, C_2. As said before these capacitances are really small. This is because they are formed by the parasitics of the transformer. C_{12} is due to the fact that the pair of windings will form a (small) capacitor. It is often called the inter-winding capacitance, connecting the primary and secondary terminals. Since both wires are made of conducting material and are separated by a dielectric material, namely air, a capacitance will form. For really high frequencies this means that a big capacitance will act as a short between these 2 terminals.

The other main capacitance in this model is C_1, C_2. This is the self capacitance of the primary (C_1) or secondary (C_2) winding, often called the intra-winding or self capacitance. Similarly to C_{12}, the wires themselves will form as a string of capacitors. When the wire is wound around the core, it will create a spiral with levels on itself. This will act as a series capacitor connection between each of the wire levels. This can be modelled as a capacitor connecting the terminal to ground.

3.4.2. Inductances

Since an inductor is nothing more than a wire wound around a (magnetic) core, there will also be inductances to model. There are 2 main inductances to model: L_{MAG1} & $L_{l1}L_{l2}$. Together they form L_1, L_2, the self inductance of the windings. L_{MAG1} represents the magnetising inductance of the transformer. This is the main part of L_1, L_2. It is the inductance dictated by the flux flowing through the core. This is also the reason there is no L_{MAG2} in the model, as the core is shared by both inductors. This means that the magnetising inductance has the same magnitude for both the primary and secondary side[38].

The second part of the self inductance, L_{l1}, L_{l2} is the leakage inductance of the inductor. This is the part of the flux which is not used. It will escape the core and will not be shared between both coupled inductors. This is also the main reason why the coupling coefficient of real coupled inductors is never greater than 1. Although the leakage is very small, it cannot be neglected, especially at high frequencies.

3.4.3. Resistance

The modelled resistances consist of 2 main parts: R_1, R_2 & R_C. R_1, R_2 are the winding resistances, or copper losses. These are the resistances of the copper wires wound around the core. The values should be very small. R_C are all the core losses. These consist mainly out of the hysteresis losses and the Eddy current losses[39]. This, in contrast to the copper losses, should be as high as possible to ensure most the current is flowing through the primary inductor.

3.4.4. Mutual inductance

Lastly there is an M above the coupled inductor. This is called the mutual inductance. This is dictated by the amount of flux shared by both the inductors. M is calculated by the formula 3.11.

4

Design Process

The design process followed an iterative, experimental methodology grounded in empirical characterisation and model validation. The methodology surrounding the measurements is explained in chapter 5. Rather than committing to a single design path, the team constructed a series of physical transformer prototypes to explore the effects of geometry, winding configuration, and conductor type. The transformer was treated as a modular product within a DC-DC conversion system, where its primary function was to handle an AC signal generated by the switching circuit.

4.1. Magnetic Cores

To operate at high frequencies the selection of core type, core material, and winding configuration play an important role. These factors influence the magnetic coupling efficiency, thermal behaviour, electromagnetic compatibility and losses.

Toroidal cores were selected over alternatives such as E-cores or planar PCB-integrated transformers for both practical and performance reasons. The toroidal shape was abundant in the lab, which reduced cost and procurement time. More importantly, the team's initial research indicated that toroids exhibit lower stray fields and EMI, making them especially well-suited to high-frequency power electronics.

The core material for the HFT transformers was chosen to be a "soft ferrite", as specified from the SMM core characteristics table 3.1. From the available toroidal cores, the following three cores were chosen:

Transformer	Ae (mm^2)	B_{max} (mT)	Material	Data sheet
Toroid Tiny (TT)	12.3	320	3E65 [40]	[41]
Toroid Medium (TM)	35.5	270	3E-10 [42]	[43]
Toroid Large (TL)	97.5	380	3C94 [44]	[45]

Table 4.1: Core materials

4.1.1. Analytical Pre-Design

A Python script, found in appendix A.1, was developed to estimate the *least* number of turns required for each design. This tool used expression 3.3 to determine the *least* number of turns for different frequency targets and core dimensions. Datasheet values for the core area and maximum flux density B_{max} (at 100°C) were used to find the minimum number of turns to avoid saturation. Inline with the programme of requirements (2.1), the voltage was set to be at $50V_{pp}$, or $35.35V_{rms}$. The tool was used both in initial and final design phases to refine the prototypes for further testing. The full table of results can be found in appendix E.2. For the desired frequency range as specified in table 2.1, see the table below: It was discovered that as the frequency increased, less turns can be used in the design.

Frequency (MHz)	TT	TM	TL
0.9	2.25	0.92	0.24
1	2.02	0.83	0.21
1.2	1.69	0.69	0.18
1.4	1.44	0.59	0.15
1.6	1.26	0.52	0.13
1.8	1.12	0.46	0.12
2	1.01	0.42	0.11
3	0.67	0.28	0.07

Table 4.2: Minimum number of turns needed per core

4.1.2. Simulation Tools

To model transformer behaviour at higher frequencies, more detailed and accurate models are required to account for the various parasitic effects and losses. These are difficult to capture using only analytical methods. Simulation tools can provide a better means to analyse, optimise and model the transformer designs before prototyping. During this project two simulation tools were used: COMSOL Multiphysics for obtaining the value of various parasitics and LTspice for circuit simulations.

LTspice

LTspice was selected for the efficient simulation environment of frequency domain responses. The resonance effects can be shown within this circuit environment and the usable frequency range can be obtained. Previous experience with this simulation tool also allowed for more efficient use.

An equivalent model of a transformer that was constructed in LTspice can be seen in figure 3.9. A sinusoidal voltage source is connected to the input of the equivalent circuit. It provides a 50-volt amplitude, as this is one of the requirements, and a 1 megahertz frequency. The model parameters were obtained from measurements 6.1, analytical methods 6.1.1, and COMSOL simulations 6.4.2. For the model the core resistance, Rc, can be ignored because the core losses in a ferrite core are low and low core losses mean a large core resistance [38].

COMSOL

COMSOL Multiphysics was used for its ability to model multiple physical environments with complex geometries. This allows, most importantly, for the finding of leakage and magnetising inductance, as well as parasitic capacitances.

As the focus lies on toroidal cores, and what was later found out windings on opposite sites are the focus 7.0.1, an almost automatic COMSOL model was created. An almost fully automated COMSOL model allows for quick changes and testing of several toroidal core sizes with different winding numbers. The only input required is the parameters of the core, wires used, and a small amount of labour, as this could not be fully automated.

First the core volume and a small insulation layer is made with their respective parameters. For configuration 1, a wire curve will be made at opposite ends of the core. The current creation can be seen below in Figure 4.1. The highlighted blue edges, the top parts of both windings, are then copied and rotated N-1 times around the core, where N is the number of times the wire is wound around the core. After all copies are connected to form a uniform path, the only non-automated part comes into play. As COMSOL creates a new model all new edges get a different label. Thus, the last outer curve for both the primary and secondary winding has to be reselected and is then placed at its original position and rotated outwards. A face is placed at the end of this curve and the entire wire is then swept. At last the wires are extended and an air box is placed around the core to simulate the air, the final can be seen in Figure 4.1b.

(a) General Toroidal Core Model

(b) 20 Turns Toroidal Core Model

Figure 4.1: Toroidal Core Model

The windings are given a copper material, with high permittivity so COMSOL recognizes it as a conductor [46]. They are densely meshed as the windings are close together and a higher accuracy is obtained. The core consists of an insulation layer of air material and a ferrite material. The mesh quality is less dense meshed compared to the wires. The air box is given the air material and is coarsely meshed as it is far away from the core and should not have a big influence on the measurements. The electrical conductivity of air and ferrite was given a non-zero value to prevent difficulties in converging. The meshed geometry can be seen in Figure 4.2. A minimum mesh quality of 0.1204 was achieved, which is sufficient for the convergence of COMSOL simulations.

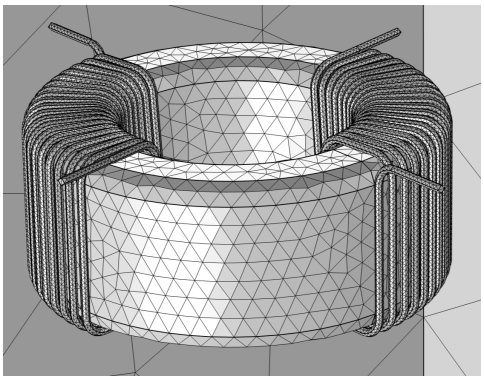

Figure 4.2: Toroidal Core Mesh

During the project it was found that a simpler geometry was required for the Magnetic Field simulations to extract the inductances, as the more complex model would take a very long time to converge. A solution is to use sheets instead of wires. This can be seen in Figure 4.3.

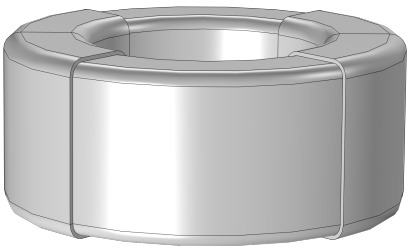

Figure 4.3: 20 Turns Toroidal Core Simplified

5

Methodology and Setup

5.1. Building the transformer

Each prototype was wound manually. To ensure consistency across builds, pliers were used to tightly wind the wire with minimal spacing between turns and close contact with the core. While exact winding tension and alignment could not be standardised, visible irregularities were minimised through visual checks and repetition.

Prototypes were grouped by core size and labelled based on conductor type and winding configuration. The TT series included 1, 2, and 3-turn copper windings, a 3-turn braided copper configuration (exploratory only), and a 3-turn layered design. The TM series included 5-turn, 10-turn, and 5-turn layered configurations in copper, as well as 5-turn windings using both thick and thin litz wire. Litz wire was only used on the medium core size and in the final design phase, based on positive results with the 5-turn medium copper prototype. The TL series included 5-turn, 20-turn, and 13-turn layered designs. 11 transformers were built and tested in the measurements phase and 2 extra transformers, using Litz wire, were built and tested in the final phase for a total of 13 transformers. See the figure below for some of the built toroids.

The copper wire used has a diameter d of 0.75mm and a resistivity of $1.68 \cdot 10^{-8}\ \Omega \cdot \text{m}$ at 20°C.

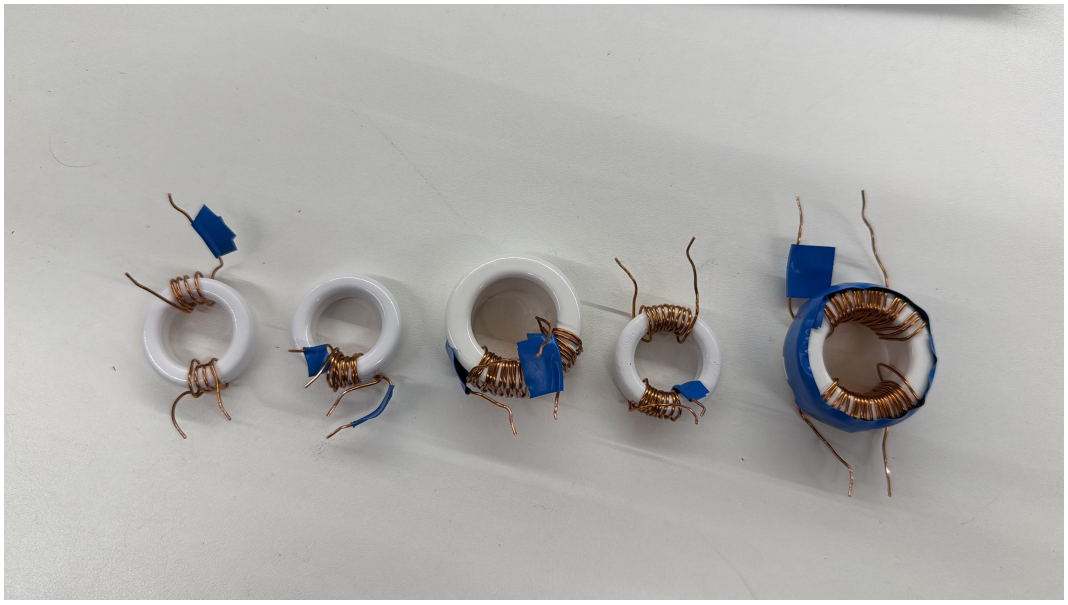

Figure 5.1: Toroids, from left to right: TM 5, TM 5 layered, TL 13 layered, TM 10, TL 20

5.2. Use of Bode 100 VNA

To help with modelling the transformer some models can be made. These models rely upon values such as inductance or capacitance to work properly. This section will tell how these values were obtained. All the measurements are done using the BODE 100 Vector Network Analyser unless otherwise specified.

The BODE 100 is a Vector Network Analyser. As shown in figure 5.2 It is a device with 3 ports. 1 port, the most left one, acts as a transmitter. While the other 2 ports act as receivers. By analysing the reflection parameters of the device which is connected to the terminals, it can find several parameters. Such as inductances, capacitances and resistances. There is a specific user manual for the finding of parameters of transformers[38].

Figure 5.2: BODE 100 VNA.

5.2.1. Inductances

In the transformer there is of course an inductance. This is due to the fact that inductors are the main component that transfer the energy from the primary side to the secondary side. This inductance consists out of two other inductances, the leakage inductance and the magnetising inductance. These inductances are in series so that $L_1 = L_{l1} + L_{mag1}$. The inductance is measured by connecting the terminals of the primary to the positive and negative terminals, while leaving the secondary side open so no current is flowing through the secondary inductor. The VNA will produce a transfer function. The primary inductance will be read where the transfer is as flat as possible. To calculate the magnetising inductance another measurement has to be done. This will be done using the 2 ports of the VNA. This will measure the overall gain of the transformer.

$$G = \frac{\omega L_{mag1}}{\sqrt{R_1^2 + (\omega L_{mag1})^2}} \cdot \frac{1}{a} \tag{5.1}$$

Where G is the measured gain of the overall system, a the turns ratio, R_1 the DC resistance of the primary winding and ω is the frequency at which L_1 was measured. By rewriting equation 5.1, the primary magnetising inductance can be calculated. Having found the magnetising inductance the leakage inductance follows from: $L_1 = L_{l1} + L_{mag1}$. This measurement can be repeated for the secondary side. However, there is a difference. Since the magnetising inductance is the flux shared by both solenoids, it is the same as the mutual inductance, there will not be a secondary magnetising inductance (L_{mag2}). The value used for L_{mag2} is the value L_{mag1} transferred to the primary side by $\frac{1}{N^2} L_{mag1}$.
Where N^2 is the turns ratio squared; since the turns ratio in this case will always be 1 the calculation is quite elementary.

5.2.2. Capacitances

For a transformer at low frequencies (< 100kHz) the stray capacitances do not play a concerning role in the transformer. However when reaching MHz frequencies they come into play and will resonate will the self inductance. This is why it is important to study and model these capacitances to insure proper behaviour of the transformer. As mentioned in section 3.4.1 there are 2 main capacitances to figure out. The self capacitance $C_{1,2}$ and the interwinding capacitance C_{12}. Both of them can be measured by using the VNA.

The interwinding capacitance is measured by shorting the primary side into the positive terminal of the coax cable, and than short the secondary side and connecting them to the negative terminal of the

coax cable. This will result in the following equivalent circuit, which allows only current to flow through C_{12}

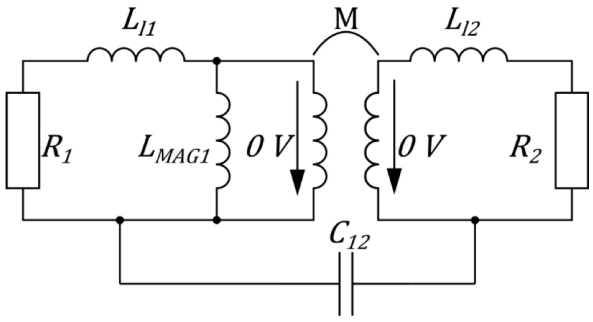

Figure 5.3: Interwinding capacitance equivalent circuit.

This measurement will produce a sweep of a user-defined frequency range. Over this range it will not be flat everywhere. The capacitance value should be read out on an area where it is as flat as possible.

For the self capacitances, only 1 port of the VNA is used. The primary terminal will be placed in the positive and negative terminals of the coax cable. The secondary side will be shorted and also be put in the negative terminal of the coax cable. Resulting in the following equivalent circuit. Where

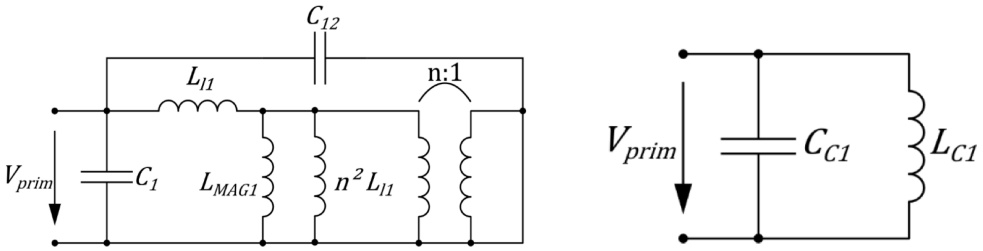

(a) Voltage curves no saturation. **(b)** Self capacitance equivalent circuit.

Figure 5.4: Self capacitance equivalent circuit.

$C_{C1} = C_1 + C_{12}$ and $L_{C1} = L_{l1} + \frac{L_{MAG1} \cdot n^2 l_{l2}}{L_{MAG1} + n^2 L_{l2}}$.
Since the inductance measurements should have been conducted before the capacitance measurement, both the leakage inductances and the magnetising inductance should be known. So L_{C1} can be easily calculated. To then find C_1 a sweep has to take place, which will read out the impedance of the system. This will provide a resonance peak at some frequency. Since the equivalent circuit is a simple LC-circuit the capacitance can be calculated by using the following relation:

$$C_{C1} = \frac{1}{\omega^2 L_{C1}} \tag{5.2}$$

This leaves only the resistance as unknown in the model.

5.3. Measuring the resistance

The DC resistance will also normally be measured using the VNA. However since the transformers consist of the least number of turns, the DC resistance will be too small to measure with the VNA. This resistance is seen as noise, producing faulty readings. This was solved by simply using a DC source. By connecting one side of a winding to the positive terminal and the other side to the negative terminal. Then passing a current through the wire, the voltage on both terminals can be measured. By applying Ohm's law the resistance can be found. In addition to this, an ohmmeter is used to verify the DC source values.

However, this is just the DC resistance. Since the transformer has to operate at MHz frequencies the resistance of a round conductor will not be the same for each frequency. This is due to the skin effect.

At high frequencies the current through a conductor tends to flow more towards the outer radius of a conductor. To find out how effective a small round copper wire at high frequency is, the skin depth has to be calculated. This can be done using the following equation:

$$\delta = \sqrt{\frac{2}{\omega\mu\sigma}} \tag{5.3}$$

The skin depth is equal to the depth the current density has been attenuated by $\frac{1}{e}$, or –8.7dB[47]. From this it is clear that the radius of the conductor, ideally, is much smaller then the skin depth. This is not usually the case for small copper wires. This will produce an AC resistance. To measure this AC resistance the idea was to hook up the VNA again and do a frequency sweep. This, however, turned out not to work. So the only indication for the AC resistance would turn out is just the theory. The ratio $\frac{R_{AC}}{R_{DC}}$ is given by the following formula:

$$\frac{R_{AC}}{R_{DC}} = \frac{\pi r^2}{\pi(2r-\delta)\delta} \tag{5.4}$$

Where r is the radius of the round conductor and δ is the skin depth.

5.4. Measuring the saturation

To validate the theory that the transformers will indeed saturate at certain voltage/current levels a setup had to be built. The easiest way was to hook a function generator to one side of the transformer and measure the voltage across it. There were, however, some difficulties with that. Firstly the RMS-voltage of some configurations were higher then what the function generator alone could handle. Secondly the current going through the inductor could not be accurately measured. This is because when measuring the voltage over the inductor, it tells something about the rate of change of the current, due to the fact that $V = L\frac{di(t)}{dt}$.

Figure 5.5: Measurement setup for core saturation.

So to fix these problems, 2 solutions were implemented. To get an accurate current reading a resistor of 2Ω has been placed in series with the inductor. The voltage can then be measured across that resistor and using Ohm's law the current can be deduced, since the current-voltage relation of a resistor is linear. To make sure the output power of the oscilloscope was enough, an amplifier has been placed

between the output of the function generator and the inductor. This made sure that a high enough RMS voltage could be produced to further study the effects of saturation. The setup can be seen in figure 5.5.

5.5. COMSOL

To measure different parameters, only two physics simulations were utilized. The first is electrostatics to measure inter- and intra-winding capacitances, and the second is magnetic fields for measuring leakage and magnetizing inductances.

5.5.1. Electrostatics

In electrostatics COMSOL utilizes Maxwell's equations in their static form for solving the simulations [48]. An important role during the simulation is Gauss's law as this allows for the surface integration of $Q = \oint_S \vec{D} \cdot \hat{n} d\vec{s}$, where Q is the free electric charge inside a closed surface, $\vec{D}$ is the electric displacement field and $\hat{n}$ is a vector pointing out of the surface. The capacitance can then be calculated by $C = \frac{Q}{V}$. The final equation used in COMSOL for capacitance calculations is then:

$$C = \frac{\oint_S \vec{D} \cdot \hat{n} d\vec{S}}{V} \tag{5.5}$$

Stationary studies were used for the electrostatic physics.

Obtaining the intra-winding capacitance C_1 will use the same setup as when measured with the VNA, 5.2.2. This is done to keep the simulated model as similar to the real measurement setup. A voltage is applied to one end of the primary winding and grounded at the other end. The secondary windings will be shorted and connected to ground. The same can be done for C_2 but then applying a voltage to the secondary winding. Surface integration is then applied on the respective winding to measure its capacitance.

The mutual capacitance will be acquired by shorting the primary winding and applying a voltage. The secondary winding will be shorted and grounded. Surface integration will be applied to the primary winding.

5.5.2. Magnetic Fields

Magnetic Fields physics also utilizes relevant Maxwell's equations. The inductance can be obtained from $L = \frac{2W_m}{I^2}$, with W_m being the magnetic energy stored in the system. The final inductance equation is a volume integration of the system:

$$L = \int_V \frac{2W_m}{I^2} dV \tag{5.6}$$

Frequency domain studies are used to measure inductances at low frequencies and a coil geometry analysis must be performed before the frequency domain study to compute the current flow in a 3D coil model. As previously explained the simplified model of the toroidal core, Figure 4.3, is used for the magnetic field simulations. Ampère's law in solids needs to be added for COMSOL to function properly during this simulation. The windings are given the homogenized multiturn property and the number of turns was specified.

To recreate the measurements done with the VNA the self-inductance is acquired by exciting the primary winding with a current and leaving the secondary winding open. The self-inductance shorted uses the same setup but with the secondary side shorted. After this the coupling factor can be calculated and consequently the magnetising and leakage inductances are obtained. The leakage inductance of the secondary winding can be obtained by swapping the setup for the primary and secondary windings. However the result should be the same because this is a 1-to-1 transformer.

6

Measurements and Calculations

6.1. Values gathered from the VNA

6.1.1. Inductances

Many VNA measurements were conducted which produced a lot of redundant parameters. To have an idea of what to work with an excel sheet had been made. In this excel sheet the most promising and stable results were added. It can be found in appendix E. This was the main source for all the values and calculations done in this chapter. The VNA graphs for frequency responses and primary inductances can be found in appendix B and C, respectively.

Primary Coil Self-Inductance

Equation (3.8) will be used to validate measured values of the primary inductance obtained experimentally using the Bode 100 VNA. The comparison serves both to confirm the accuracy of the measurements, as well as a tool to assess the consistency of the core's magnetic parameters. The values for the calculated primary inductance are compared to the measured values in the table below:

Core, Windings, Config.	Calculated L_1 (μH)	Measured L_1 (μH)	Percentage error (%)
TT, 1, 1	2.30	2.78	+20.93
TT, 2, 1	9.19	9.13	–0.61
TT, 3, 1	20.68	19.03	–7.94
TT, 3, *braided*	20.68	19.77	–4.35
TT, 3, 2	20.68	20.85	+0.87
TM, 5, 1	152.36	158.76	+4.20
TM, 10, 1	609.43	643.39	+5.57
TM, 5, 2	152.36	91.36	–40.04
TL, 5, 1	78.50	84.50	+7.64
TL, 20, 1	1260.00	1326.00	+5.57
TL, 13, 2	530.66	502.44	–5.32

Table 6.1: Calculated values of L_1 compared to the measured values of L_1

In general, the measured inductance values correspond well with the calculated theoretical predictions, with deviations within 8% for the majority of samples. The lowest percentage error is –0.61% for *TT, 2, 1*. The largest *non-outlier* percentage error was found to be –7.94% for *TT, 3, 1*. It is clear, however, that two measurements (*TT, 1, 1* and *TM, 5, 2*) exhibit significant deviation from their calculated values, with errors of +20.93% and –40.04%, respectively. These two measurements are considered outliers since they deviate more than 10% from the theoretical prediction. *TT, 1, 1* is believed to deviate due to the sensitivity of the Bode 100 VNA device. During the measurement phase, it was noted that any slight movement in the coaxial cable connected to the transformer would cause large deviations in data. For this reason, the sample is considered faulty and will be redone further in section 6.1.1. After careful

inspection of *TM, 5, 2*, it was evident that the toroidal core possessed a crack, as can be seen in figure 6.1.

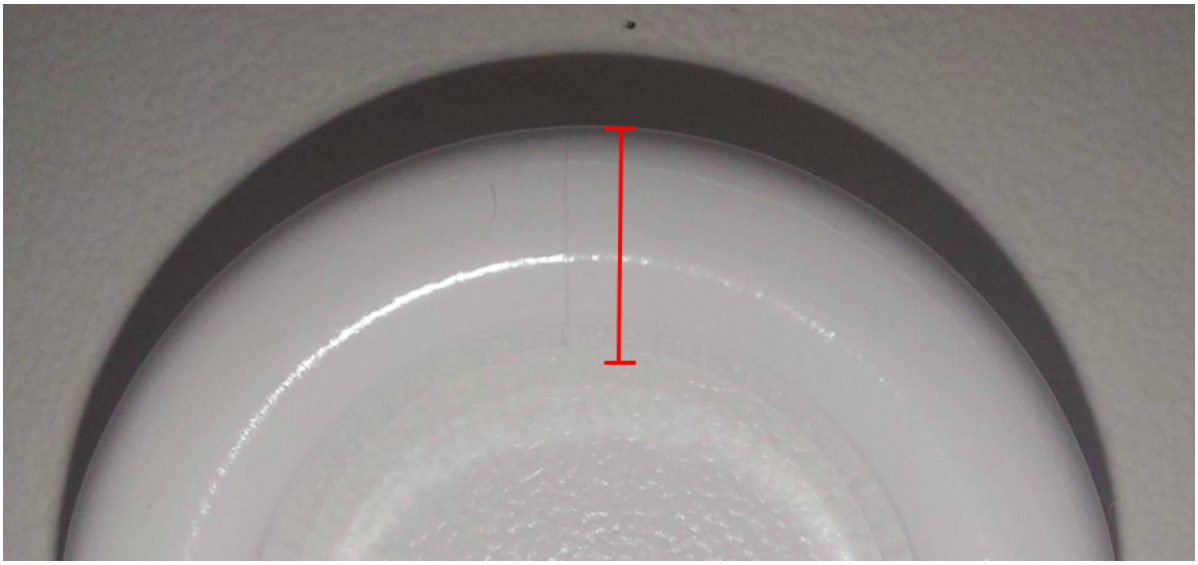

Figure 6.1: Crack in the medium toroidal core

This crack effectively created an air gap in the toroidal core. With the introduction of a gap of length g, the total reluctance increases:[49]

$$\mathcal{R}_{\text{total}} = \mathcal{R}_{\text{core}} + \mathcal{R}_{\text{gap}} = \frac{l_c}{\mu_r \mu_0 A_c} + \frac{g}{\mu_0 A_c} \tag{6.1}$$

The air gap has a relative permeability $\mu \approx 1$, and therefore $\mathcal{R}_{\text{gap}}$ is much larger than that of the ferrite core. A large increase in $\mathcal{R}$ in expression (3.8) will significantly decrease L_1, explaining the –40.04% deviation from the calculated value.

Secondary Coil Self-Inductance

The same procedure for measuring the secondary coil self-inductances is used as for the primary coil. The Bode 100 VNA is connected to the transformer and an one-port impedance measurement is taken. Since the primary and the secondary side have the same number of coils and the same expression is used 3.8, the calculated L_2 will be the same as the calculated L_1.

Core, Windings, Config.	Calculated L_2 (μH)	Measured L_2 (μH)	Percentage error (%)
TT, 1, 1	2.30	2.74	+19.13
TT, 2, 1	9.19	9.14	–0.54
TT, 3, 1	20.68	20.84	+0.77
TT, 3, *braided*	20.68	19.82	–4.35
TT, 3, 2	20.68	20.70	+0.10
TM, 5, 1	152.36	158.16	+3.81
TM, 10, 1	609.43	641.62	+5.28
TM, 5, 2	152.36	91.54	–39.92
TL, 5, 1	78.50	83.91	+6.89
TL, 20, 1	1260.00	1310.00	+3.97
TL, 13, 2	530.66	494.00	–6.91

Table 6.2: Calculated values of L_2 compared to the measured values of L_2

The values are as expected. L_1 and L_2 are expected to be similar because the number of turns and wire gauge remain unchanged. The largest deviations still lie with *TM, 5, 2* and *TT, 1, 1*, having percentage errors of –39.92% and +19.13% respectively. For both toroids the reasons for deviation is believed to

be the same reason described in the paragraph above, and re-runs of the measurements can be found below.

Redo TT, 1, 1 and TM, 5, 2

Measurements are repeated for the toroid configurations *TT, 1, 1* and *TM, 5, 2*. The copper wire gauge is kept the same, the windings are wound using similar methods and in arrangements comparable to the original transformer and the measurements are taken in the same manner. This is to ensure consistency between data points. Table 6.3 has calculated values for L, measured values for L_1 and L_2, and the associated percentage errors.

Config.	Calculated L μH	Measured L_1 (μH)	Measured L_2 (μH)	% Error L_1	% Error L_2
TT, 1, 1	2.30	2.32	2.16	–0.87	6.09
TM, 5, 2	152.36	151.38	154.23	0.64	–1.23

Table 6.3: Redo measurements of TT, 1, 1 and TM, 5, 2

Magnetising and Leakage Inductances

The magnetising inductance of the primary coil was calculated using the formula given in the Bode 100 - Application Note [38], which in turn is a rearrangement of equation 5.1.

$$L_{mag1} = \frac{Ga}{\omega}\sqrt{R_1^2 + (\omega L_1)^2} \tag{6.2}$$

Again, ω is the frequency at which L_1 and the gain G were measured, a the turns ratio (= 1). The magnetising inductance of the secondary coil was calculated using equation 6.3 [38]:

$$L_{mag2} = L_{mag1} \cdot (\frac{N_2}{N_1})^2 \tag{6.3}$$

Where N_2 is the number of turns on the secondary side and N_1 the number of turns on the primary side. Since the turns ratio is 1, the fraction on the right is simply 1 and the magnetising inductance in the secondary coil is the same as the magnetising inductance in the primary coil. Therefore:

$$L_{mag1} = L_{mag2} = L_{mag} \tag{6.4}$$

The leakage inductance can be calculated using expression 3.15. Rearranging for L_l:

$$L_l = L - L_{mag} \tag{6.5}$$

The values for L_{mag}, L_{l1}, L_{L2} are as follows:

Core, Windings, Config.	Calculated L_{mag}(μH)	Calculated L_{l1}(μH)	Calculated L_{l2}(μH)
TT, 1, 1	2.44	0.338	0.305
TT, 2, 1	8.74	0.394	0.404
TT, 3, 1	18.59	0.433	2.24
TT, 3, *braided*	19.47	0.3	0.332
TT, 3, 2	20.64	0.205	0.059
TM, 5, 1	157.49	1.27	0.667
TM, 10, 1	639.24	4.15	2.38
TM, 5, 2	91.10	0.256	0.438
TL, 5, 1	82.57	1.92	1.34
TL, 20, 1	1307.05	18.95	2.95
TL, 13, 2	502.25	0.194	5.00

Table 6.4: Calculated values of L_{mag1}, L_{l1}, L_{L2}

Preliminary research [9] in section 3.1.4 predicted that layering the coils over each other would reduce the leakage inductance. This behaviour is seen when comparing *TT, 3, 1* with *TT, 3, 2* and *TM, 5, 1*

with *TM, 5, 2*. For *TT, 3 turns*, having the coils layered decreased L_1 by 52.66% and L_2 by 97.36%. For *TM, 5 turns*, L_1 decreased by 79.84% and L_2 by 34.33%. Unfortunately, the percentage decreases are not consistent between measurements. It *can* be said that the leakage inductance does indeed decrease if the coils are layered, however the *exact* effect of said configuration cannot be stated. Only 1 measurement was taken, limiting the validity of the results.

6.1.2. Coupling Factor

The coupling factor was calculated with two measured values - the self-inductance and the self-inductance shorted, [38].

$$k = \sqrt{1 - \frac{L_s}{L_1}} \tag{6.6}$$

Where L_s is the inductivity measured at the primary winding of the transformer, with shorted secondary winding. Results are given in the table below.

Transformer	Coupling factor k
TT, 1, 1	0.878
TT, 2, 1	0.957
TT, 3, 1	0.977
TT, 3, *braided*	0.985
TT, 3, 2	0.990
TM, 5, 1	0.992
TM, 10, 1	0.994
TM, 5, 2	0.997
TL, 5, 1	0.977
TL, 20, 1	0.986
TL, 13, 2	0.999

Table 6.5: Coupling factors of different transformers

6.2. Resistances

6.2.1. DC Resistance

The DC resistance of a conductor can be calculated by using the following relation:

$$R = \frac{\rho l}{A} \tag{6.7}$$

Where ρ is the resistivity of the conducting material, with units [$\Omega \cdot$ m]. This makes perfect sense, since the electrical current will face less resistance when flowing through a bigger surface. The current will face more resistance if the conductor is longer because it has more material to traverse.

Core size + N	R calculated (mΩ)	R measured (mΩ)	Difference (%)
TT 1	3.01	4.20	-28.22
TT 2	3.69	4.20	-12.20
TT 3	4.36	4.30	1.42
TB 3	4.36	4.12	5.85
TM 5	7.90	6.45	22.52
TM 10	13.5	11.5	17.17
TL 5	11.5	11.5	0.36
TL 20	39.1	37.4	4.58

Table 6.6: Wire DC resistances calculated versus measured.

These values were calculated by taking the length of the wires as long as the circumference of each respective core. Since the wires do not end immediately after the circumference of the core, as this would oppose some issued connecting the core to the circuit, a buffer has been added of 3cm. Having

done all the calculations using equation 6.7. They can be found in table 6.6. These values are pretty accurate with differences ranging from 0.36% to 28.22%. The inaccuracies will be mainly be caused by the endings of the wires. Since not all wires have a buffer of exactly 3cm. Some toroids will have longer ending and other will have smaller endings. But overall it can be assumed that the resistance equation is rather accurate and could be used for prototyping.

6.2.2. AC Resistance

In addition to calculating and measuring the DC resistance, a python script was written to theoretically calculate the AC resistance. This is done using equation 5.4 and a modified version of equation 6.7. Initially, equation 5.4 was plotted between 1Hz and 4MHz for a copper wire of length 20cm and diameter 0.75mm.

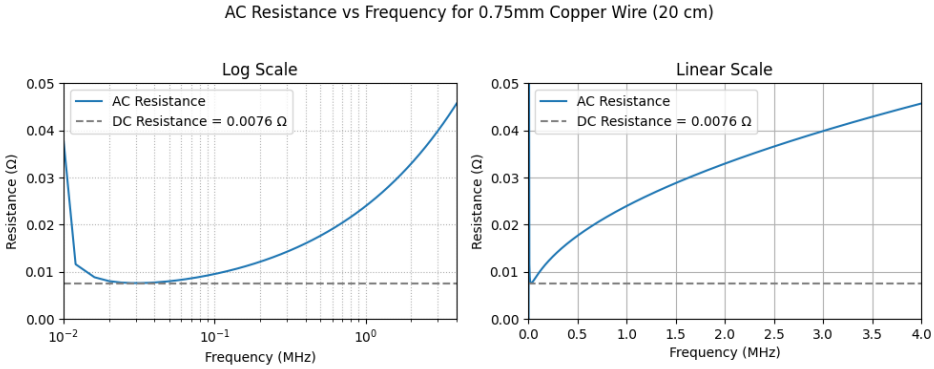

Figure 6.2: AC resistance graph as a function of frequency

There is some odd behaviour. At very low frequencies, the AC resistance spikes. This is because the skin depth becomes larger than the wire radius at low frequencies, causing the denominator to artificially shrink. To solve this issue, a smooth transition is implemented with equation 6.8.

$$R_{AC} = R_{DC}\sqrt{1 + \frac{R_{skin}}{R_{DC}}} \tag{6.8}$$

Where R_{skin} is now equation 5.4. This ensures that at low frequencies $R_{AC} \approx R_{DC}$ and at high frequencies $R_{AC} = R_{skin}$.

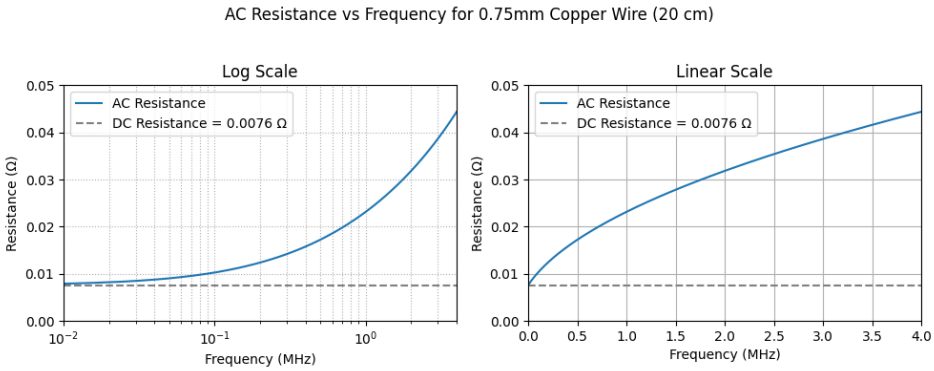

Figure 6.3: AC resistance with smoothing

Figure 6.3 has the smoothing implemented. Here we see that at higher frequencies the AC resistance increases, therefore increasing losses in the transformer. At 1.5MHz the AC resistance is $\approx 4\times$ larger

than the DC resistance. Litz wire use is recommended at high frequencies - it reduces the AC resistance as it is a bundle of copper wires with tiny radius', decreasing skin depth and skin effects.

6.2.3. Capacitances

Using the VNA, as described in section 5.2.2, the interwinding and intrawinding capacitances were measured. Table 6.7 shows these values.

Transformer	Interwinding C (pF)	Intrawinding C_1 (pF)	Intrawinding C_2 (pF)
TT, 1, 1	1.33	36.0	36.4
TT, 2, 1	1.40	36.7	42.1
TT, 3, 1	0.001	13.3	15.2
TT, 3, *braided*	10.0	15.7	15.6
TT, 3, 2	6.00	38.4	32.6
TM, 5, 1	3.13	62.9	63.1
TM, 10, 1	15.8	46.2	46.3
TM, 5, 2	11.0	3.68	3.65
TL, 5, 1	5.18	2.02	0.425
TL, 20, 1	15.7	88.1	89.4
TL, 13, 2	43.0	3510	3610

Table 6.7: Measured capacitances using the VNA

Some measurements appear wrong or vary greatly as compared to other results. *TT, 3, 1* has an interwinding capacitance that is a lot lower than the other Tiny Toroids, and it is believed that this is due to a wrong measurement. The same can be said for the intrawinding capacitance of *TM, 5, 1*. The intrawinding capacitances for *TL, 13, 2* are really big.

6.3. COMSOL Values

6.3.1. Capacitances

The capacitances were both calculated and measured. The measurements were done by the VNA. For the calculation of the interwinding capacitance some assumptions were made. Mainly the wires were assumed to be a plate, around the transformer. As shown in figure 6.4 By using this assumption the

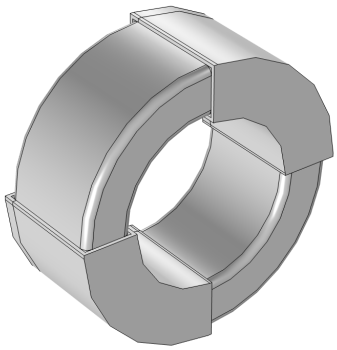

Figure 6.4: Model for capacitance calculations.

capacitance between the 2 winding can be done by using the capacitance equation: $C = \varepsilon \frac{A}{d}$. Where A is the area, ε is the permittivity of the material between the plates and d is the distance between the plates. The distance between plates is also an estimation. For the cores with a small amount of turns (≤ 5) the distance between the winding will just be measured. For those with more windings it will be calculated by finding the average length to the middle of the core using:

$$d = \frac{1}{T} \int_{-\frac{T}{2}}^{\frac{T}{2}} r \cos(x) dx \tag{6.9}$$

Where r is the inner radius of the core minus the wire thickness. T is the length in radians which the wires cover. So for example in figure 6.4 T = $\frac{\pi}{2}$.

Core size + N	Measured capacitance (pF)	Calculated capacitance (pF)	Difference (%)
TT 3	0.001	0.00866	766
TM 5	3.13	0.0363	-98.9
TM 10	15.8	0.0708	-99.4
TL 5	5.18	0.0392	-99.04
TL 20	15.7	0.243	-98,3

Table 6.8: Measured and calculated capacitance

The area is calculated by simply multiplying the width times the length. In reality some fringing will also occur. To incorporate this effect, 2 times half the height of the core has been added. The length is taken to be the arc length of the inner core for N > 5. The angle in radian differed for the cores with N > 5. For the TM 10 θ = $\frac{\pi}{4}$ and for TL 20 θ = $\frac{\pi}{2}$. As seen in table 6.8 there are some big discrepancies between the actual value and the calculated values. This was due to the effect of the core. Because the core had a larger permittivity than air the capacitance would be a lot bigger than if there was no core. This can be clearly seen in the results. If the core was removed the measured capacitance values would tend more towards the calculated capacitance values.

A method for calculating the self-capacitance with a core was found in chapter 9.15 from [9]. However more discrepancies arose, thus capacitance calculations were deemed difficult to calculate and would be solved with COMSOL.

6.4. Simulations

6.4.1. LTSpice

Using the values obtained earlier the equivalent circuit of the transformer model, from Figure 3.9, is filled in. For the large toroid of configuration 1 with 20 turns this will result in Figure 6.5. The only discrepancy between this circuit and the obtained values is the leakage inductance of the secondary side, which is changed from 2.95μH to 19μH. As the transformer is 1-to-1 the wire resistance, intra-winding capacitance and leakage inductance should have the same values for primary and secondary windings. The value of 19μH is used for the leakage as this value is the closest to 20.1μH, which is obtained from COMSOL simulations 6.4.2.

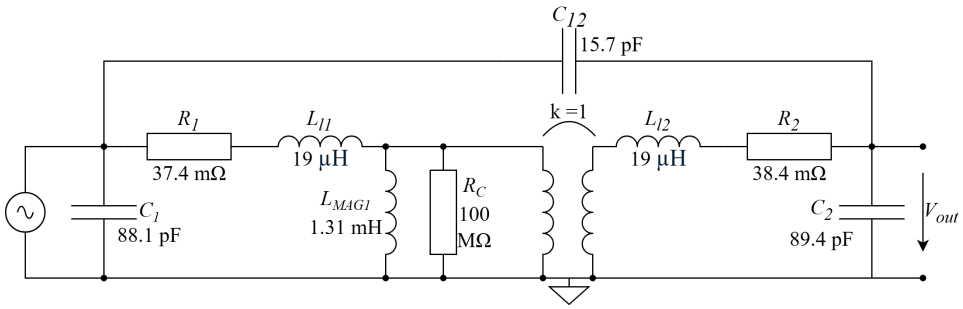

Figure 6.5: LTspice circuit

An AC analysis sweep from 1 to 50 megahertz will be used, as this is the frequency range measurable with the VNA. Measuring the gain phase figure 6.6a is then obtained. The first resonant peaks are the most important as they determine the usable frequency range. In Figure 6.6b the VNA gain-phase simulation plot can be seen.

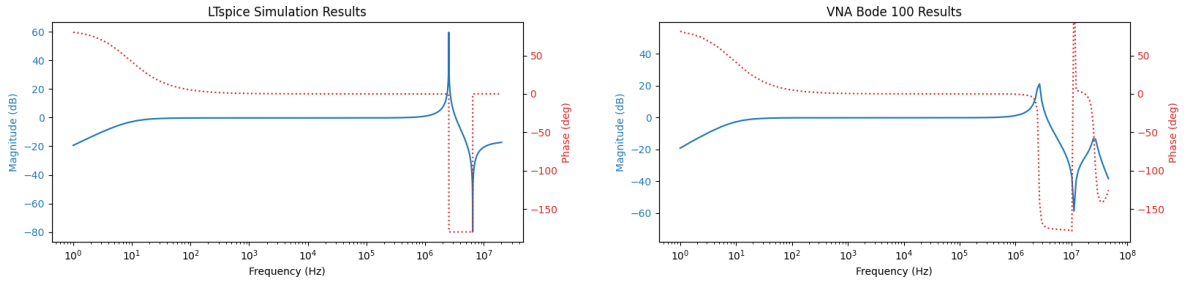

(a) LTspice simulation

(b) VNA simulation

Figure 6.6: Toroidal Core - Configuration 1 - 20 Turns - Gain-Phase Simulation

The resonance frequency peaks of the LTspice simulation can be seen at 2.5MHz and 6.49MHz, where the VNA simulation has peaks at 2.6MHz, 11MHz and 25MHz. The first resonant peaks correspond between LTspice and the VNA simulation. The most important thing to note is the third peak, which doesn't show in the LTspice simulation. The probable cause is due to the core's behaviour at around this frequency range. Because the core is not taken into account for the LTspice simulations it doesn't show this behaviour. This can also explain the discrepancy between the second resonant peaks of the simulations, as this is influenced by the secondary and mutual capacitance values. Because the first resonant peak is the most important, as this determines the usable frequency range the LTspice model can simulate and result in the usable frequency range of the transformer.

6.4.2. COMSOL

Capacitances

The parameters that are measured earlier in this chapter can now be used to create a COMSOL model that can simulate the behaviour of the core. First the electrostatic simulation setup is used to calculate the parasitic capacitances, 5.5.1. Figure 6.7a shows the linear gradient of voltage going through the winding for the self-capacitance measurement. Figure 6.7b shows the voltages applied to one side and the other grounded

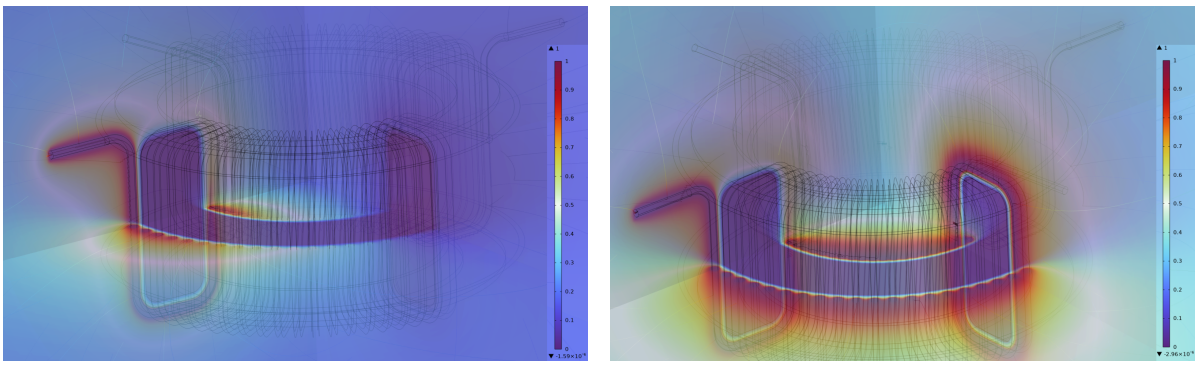

(a) Self-Capacitance Simulation

(b) Mutual Capacitance Simulation

Figure 6.7: Toroidal Core - Configuration 1 - 20 Turns - COMSOL Electrostatic Simulations

Doing surface integration of equation 5.5, $C = \frac{\oint_S \vec{D} \cdot \hat{n} d\vec{S}}{V}$, the obtained self-capacitance value is 85.938pF and mutual capacitance value is 14.018pF. Comparing this with the self-capacitance value from the VNA being 88.1pF and the mutual capacitance from the VNA being 15.7pF, it seems like the COMSOL model can correctly evaluate the parasitic capacitance values with a small discrepancy. Simulation of the mutual capacitance without a core, it was chosen as air, resulted in a large change in the capacitance. The mutual capacitance obtained with an air core resulted in a value of 0.971pF, compared to the 14.018pF is a large difference. This might be the reason for the earlier faulty calculations of the mutual capacitance, 6.3.1, because that was done without consideration of the core.

Inductances

Using the magnetic field physics the self-inductance and self-inductance shorted can be found by volume integrating using equation 5.6, $L = \int_V \frac{2W_m}{I^2} dV$, over the volume. After the simulation, Figure 6.8a is obtained for the self-inductance and Figure 6.8b for the self-inductance shorted, they both show the magnetic flux density going through the core. The most noticeable point of these simulations is that the magnetic flux does go through the entire core when the second winding is left open and that there becomes a linear gradient when the secondary winding is shorted. This is as expected because when the secondary winding is left open there will be no current flowing through this winding and thus no influence from this winding on the magnetic flux density. Shorting the secondary winding allows for a current to flow which generates a magnetomotive force that counteracts the magnetic flux density created by the primary. This effect is shown by the gradient of this figure.

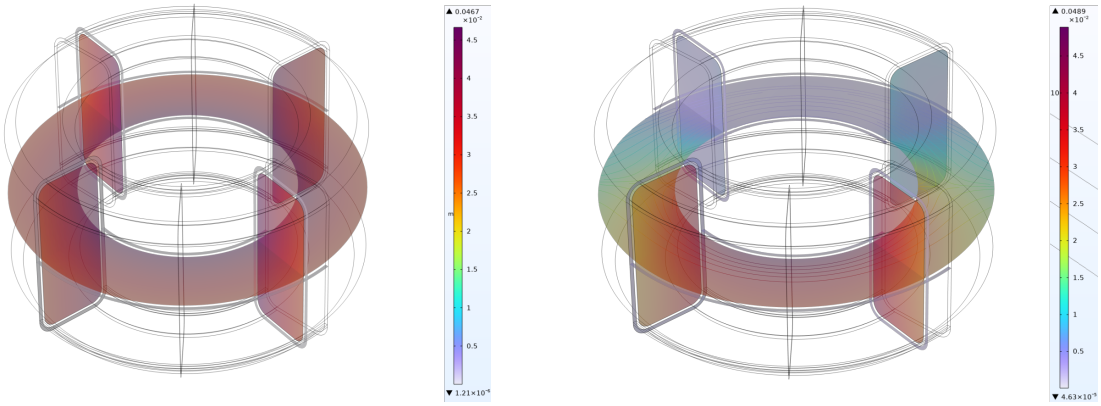

(a) Self Inductance

(b) Self Inductance Shorted

Figure 6.8: Toroidal Core - Configuration 1 - 20 Turns - COMSOL Magnetic Field Simulations

Using the volume integration from equation 5.6, $L = \int_V \frac{2W_m}{I^2} dV$, results in a self-inductance value of 1.4233mH and a self-inductance shorted value of 39.841μH. Compared to the measured values from the VNA being 1.33mH, for the self-inductance, and 37.6μH for the self-inductance shorted. It seems like the model can evaluate the self-inductance values. Using equation 6.1.2 for the coupling factor, equation 6.1.1 for the magnetising inductance, equation 6.1.1 for the leakage inductance and also having the measured resistance value from 6.2. The calculated COMSOL values become 1.4mH for magnetising inductance and 20.1μH, compared to the values calculated from the VNA being 1.31mH and 19μH respectively. These values are close enough to conclude that COMSOL can be used for optimizing and comparing with the measured values.

6.5. Saturation

6.5.1. Oscilloscope and Amplifier

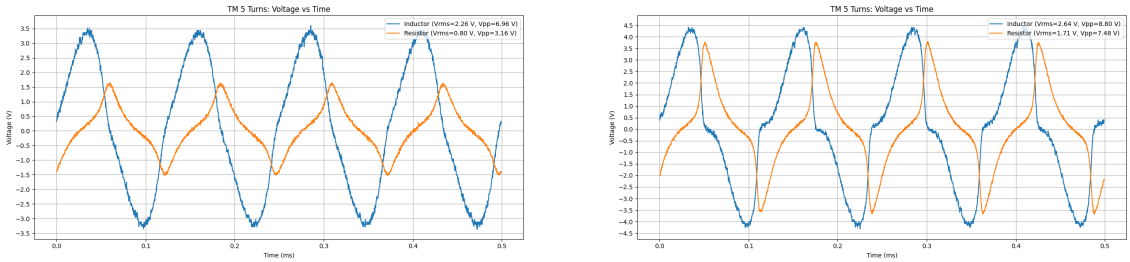

(a) Voltage curves no saturation.

(b) Voltage curves in saturation.

Figure 6.9: Voltage curves during and before saturation occurs.

Once the setup was completed for the measuring of the saturation, measurements were conducted. The results of which can be seen in table 6.9. The reason why only the voltage can be seen in figure 6.9a is primarily due to the fact that the fundamental transformer equation relates the maximum voltage a transformer can handle before saturating. However the current was also monitored. As the resistor had a value of 2Ω, the current could easily be deduced from Ohm's law with the values of the graph.

Core size + N turns	frequency (kHz)	Calculated $V_{sat-rms}$ (V)	Measured $V_{sat-rms}$(V)	% difference
TL 5	10	10.3896	8.15	–21.5
TL 20	4	16.62336	11.89	–28.47
TT 3	30	2.3100876	1.97	–14.72
TT 1	50	1.283382	0.95	–25.98
TM 5	8	2.900208	2.64	–8.97

Table 6.9: Measurement data for the core saturation.

$V_{sat-rms}$ was calculated using formula 3.3. Where the number of turns and magnetic area of the core were constants. The frequency range was rather limited due to the fact that the effective range of the amplifier had a limit of 50kHz. The transformer had a bandwidth which started at around 1kHz. This means that the calculations had to be done using lower frequencies then the eventual operating frequency of the transformer. Important to note is that these measurements were done mainly to validate the EMF equation. If the equation holds then it should also hold for higher frequencies which will help with prototyping. It is nice to see that the experimental setup follows the theoretical values, to some degree. It can be seen that the error is between $\approx 9-30\%$, which is a pretty large error still. An explanation for this discrepancy is that it is pretty unclear at what point the saturation actually occurs. As seen in figure 6.9a there already is a light form of saturation happening, but in figure 6.9b it is clearer. So what plot corresponds better to the theoretical value?

That is not known for sure, however, the calculated values did correspond better to the heavier saturation which can be seen in figure 6.9b. So it can be only assumed that the calculated saturation is only valid for the bigger saturation plots. Another explanation can be that the oscilloscope did the calculation for the RMS voltage. Since the voltage wave is not purely sinusoidal, meaning that the oscilloscope might have some problem calculating the RMS value. This could result in a higher or lower value then it actually is.

It is also interesting to note that the voltage over the inductor leads the voltage across the resistor. This can be explained many ways, in this report it will be explained by using the voltage-current relation of an inductor in frequency domain. This will equate to:

$$V = j\omega Li \tag{6.10}$$

This means that for the same current wave going through both the resistor and inductor, the voltage in the inductor will lead the voltage in the resistor by $\frac{\pi}{2}$. Because when filling in equation 6.10 the voltage is purely imaginary while the voltage in a resistor in in phase with the current.

After all these measurements it is safe to assume that the EMF equation from 3.3 is valid. However is should be noted that a margin of 30% should be considered for prototyping. Just to make sure that for a certain drive power the core will not saturate. Having validated the theory of the EMF equation from 3.3, a prototype can be made considering the drive voltage and/or current. This will eliminate any uncertainty regarding the saturation of the core at higher power, frequency or current.

6.5.2. Saturation Current

Following the voltage saturations, the current at which the core saturates can be measured. A 2 ohm resistor was soldered in series, and the voltage was measured across both the resistor and the inductor coil. The peak current is calculated using formula 6.11 below, and findings are in table 6.10.

$$V_{PP} = 2 \cdot V_{peak} \Rightarrow I_{peak} = \frac{V_{pp}}{2R} \tag{6.11}$$

Where R = 2 and V_{pp} is the peak-to-peak voltage *during* saturation. Values are taken from the graphs in appendix D.

Core + Turns	Measured V_{PP} across R (V)	Measured I_{peak} (A)
TT 1	5.84	1.46
TT 3	3.72	0.93
TM 5	7.48	1.87
TL 5	7.84	1.96
TL 20	8.64	2.16

Table 6.10: Saturation currents calculated using equation 6.11

From table 6.10 it is clear that this transformer will not work properly at the specified driving capabilities of 2A/50V, as it will saturate already at 1.46A. However, this test was conducted using an amplifier. This amplifier had a limited bandwidth up to 50kHz. At lower frequency it is expected to have a lower saturation voltage/current because it is frequency dependent, this follows from the EMF equation. Since the saturation voltage is inversely proportional with the frequency as can be seen in 3.3. For prototyping all the variables from equation 3.3 will be taken into account so that the prototype cores will not saturate at the desired frequency and driving voltage/current of 2A/50V.

7 Integration

The final design of this project involves not only a transformer, but also a switching circuit driving the transformer. The group in charge of the switching circuit is using a GaN driven LLC circuit, for which the leakage of the transformer is an important variable in having a functional switching circuit. Trends revealed during the measurement phase will also be discussed.

7.0.1. Prototyping

For the prototyping stage, all previous measurements and validations come in to play.

Transformer	L_1	L_{l1}	$\frac{L_{l1}}{L_1}$ (%)
TT 3	1.90E – 05	4.33E – 07	2.28
TM 5	9.28E – 04	1.27E – 06	0.13
TM 10	6.43E – 04	4.15E – 06	0.64
TL 5	8.45E – 05	1.92E – 06	2.28
TL 20	1.33E – 03	1.90E – 05	1.43
Average			1.352

Table 7.1: Ratio leakage/self inductance

Table 7.1 shows the ratio between the (measured) self inductance and the corresponding leakage inductances. A very important distinction to make is that all these transformers were setup in the first configuration, as the switching group requested higher leakage inductance values than expected, and were only achievable through use of configuration 1 (The specified values can be found in table 7.2). From table 7.1 it is clear that the average leakage for a toroidal core in configuration 1 is around 1.352%. Taking the average over *all* the transformers tested, the average leakage was found to be 1.467% of the self-inductance.

As indicated by figure 7.1 below it can be seen that the core (TM5) will not saturate at the operating voltage of 100V. The values from the graph are determined by using the EMF equation 3.3. The blue curve is the maximum voltage limit before core saturation at different frequencies, while the turn number stays constant at 5. The grey curve represents same, but with the 30% error needed to be taken into account as explained in section 6.5.1. From this it is clear that the prototype can work well within the conditions set by the programme of requirements.

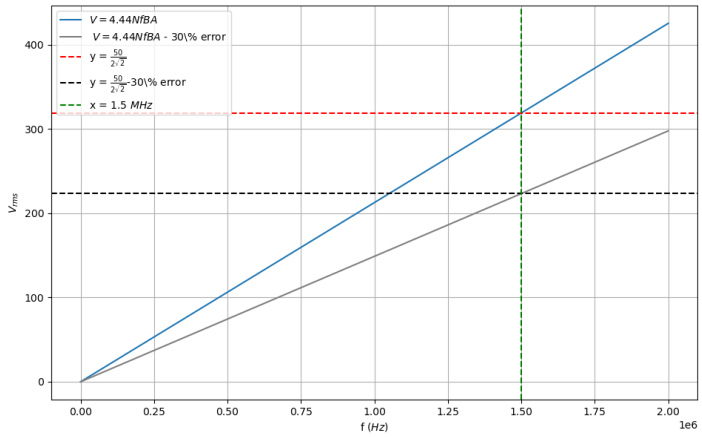

Figure 7.1: Saturation voltage of the core at 1.5MHz.

7.0.2. Trends

The many measurements conducted reveal trends useful for prototyping. A closer look was taken at the values, especially on what effect different core configurations have on values. 2 geometrical parameters dictated the differences: the number of windings per core and the core size. When the number of turns increased, there were a few noticeable changes - mainly to the winding resistance, inductances and capacitances.

Number of windings

When increasing the number of turns the resistance had a tendency to increase. This can explained by equation 6.7, where it can be seen that $R \propto l$. Meaning that for a wire constructed of the same material and same radius, the resistance increases linearly proportional to l. This matches with what is seen in the measured values.

Another thing that increased with an larger number of turns is the inductance. This can be explained by looking at equation 3.8. Here $L \propto N^2$. Consequently, an increase in turns will quadratically increase the inductance. This is best seen in the values for L_1 for *TT, 1, 1*, *TT, 2, 1* and *TT, 3, 1*. At one turn $L_1 = 2.78$, at two turns $L_1 = 9.13$ and at three turns $L_1 = 19.03$. If the quadratic relationship holds, then $L = kN^2$ for some constant k.

$$\begin{aligned} N = 1 : k = \frac{L}{N^2} = \frac{2.78}{1^2} = 2.78 \\ N = 2 : k = \frac{9.13}{2^2} = 2.28 \\ N = 3 : k = \frac{19.03}{3^2} = 2.11 \end{aligned} \tag{7.1}$$

The values of k are close but not identical. This suggests some deviation from ideal behaviour, possibly due to parasitics or imperfect coupling factor, but it *approximately* supports a quadratic trend.

Lastly there was a change noticed in the capacitances. The inter-winding capacitance increases as the number of turns increase. This can be explained by the simplification made in section 6.3.1. As the number of turns increase the ”capacitor” area increases. As shown in equation for capacitance, $C \propto A$. Therefore, if the area increases, so will the capacitance. The peculiar thing, however, is that different behaviour is observed for the intra-winding capacitances. They had a tendency to decrease as the number of turns increased. One explanation for this is the fact that for each pair of turns a ”new” capacitor is formed. When the number of turns increased, and consequently the number of pairs, there will be more capacitors. The difference, however, is that these capacitances are placed in series. The series capacitance can be calculated as follows: $\frac{1}{C_{tot}} = \frac{1}{C_1} + \frac{1}{C_2}$. So increasing the total number of capacitors in series ultimately leads to a decrease in the total capacitance.

Core size
As mentioned before, the other cause of differences was the change in core size. If the number of turns stayed constant, but dimensions such as core magnetic effective area and mean magnetic path length increased, then the inductance would decrease - Since $L \propto \frac{A_c}{l_c}$. So if the total inductance decreased it can be assumed the decrease in permeability in combination with an increase in path length is greater than the increase in area, resulting in a lower total inductance.
Additionally, a larger core meant the path length of the wire increased, leading to more resistance, corresponding with the findings. For a larger core with the same number of turns the interwinding resistance would increase.
The same logic can be applied to the capacitance since $C \propto \frac{A}{d}$. It can be assumed that an increase of core dimensions, the area will scale more than the distance between the windings, thus resulting in a larger capacitance for a bigger core. Important note is that the area when talking about the inductance is the effective area of the core. While talking about the area for the capacitance, it is the area of the windings simplified to a plate.

As for the intra-winding capacitance - it would not follow the same rules as in section 7.0.2. This could have multiple explanations, but the most probable one is that the windings were not as perfectly and tightly wound as possible. This will have great impact on the already very small capacitances. This is further backed by the fact that for all the other cores the intra-winding capacitance of the primary and secondary sides had values close to each other. For the TM5, however, the primary and secondary intra-winding capacitance were pretty far off of each other. Meaning that this spotted trend was not reliable and could not be trusted, and was most likely caused by a faulty measurement.

7.0.3. Leakage inductance matching
Having found the average leakage inductance it is now easy to design a prototype for the switching circuit. The values needed were specified within a range, meaning that there an exact value is not necessary, giving leeway in the prototyping.

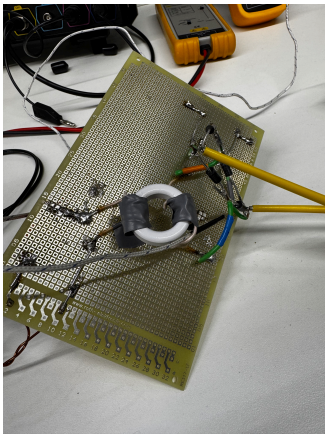

Figure 7.2: TM 5 integrated with the switching circuit.

7.0.4. Testing
Initially, the switching circuit needed a leakage inductance of $1.29\mu \leq L_{l1} \leq 2.58\mu$. To get a leakage which fits in that range the self inductance can be estimated as $\frac{L_{l1}}{0.01467}$. Resulting in $87.9\mu \leq L_1 \leq 176\mu$. Using equation 3.8 the amount of turns can be calculated specific to the size of the cores. For each of the 3 cores a winding number N was calculated:

Specific leakage wanted	TT turns	TM turns	TL turns
1.29μ	6.19	3.80	5.29
2.58μ	8.75	5.37	7.48

Table 7.2: Number of turns for specific leakage

2 transformers were built to test the theory for the leakage: the tiny core and the medium core. The tiny was built with 6 turns, while the medium was built with 5 turns. Having measured both self inductances of the transformers, they could be compared to the theoretical values. For the TT transformer $L_1 = 77\mu H$ and for the TM transformer $L_1 = 162\mu H$. Doing all the VNA calculation as described in section 5.2. This gives a leakage for the small core $L_{l1} = 0.93\mu H$ and for the medium core $L_{l1} = 2.72\mu H$.

8

Discussion

The project yielded a number of technical and methodological successes. Firstly, key behaviours predicted during the early analytical stages were confirmed in experimental results. For example, leakage inductance was reduced through layering the windings, and calculated self-inductance values matched measurements within 10% error. Two clear outliers were identified and explained, reinforcing confidence in the overall method. Other methods, for example the saturation voltage measurements and resistance measurements proved to have larger error of up to 30%. For the saturation voltage this is believed to be due to human error and capturing the wrong saturation point, while for the resistances the error lies in not having accurate lengths for the wire. Another outlier which was identified was the capacitance calculation, which was almost 100% off. This was due to the effect of the core. While having a permittivity larger than that of air, the charge accumulated would increase while remaining at the same potential. This means that with a conductive core, with a bigger ε will result in a larger capacitance. If the core was removed and than again measured it would follow the equations and simplifications more accurately. Among the prototypes, the medium-sized toroid with five turns emerged as the best-performing design relative to the system specification. This was subsequently re-prototyped using Litz wire, which further improved performance, particularly under MHz-range operation. The VNA proved effective for measuring inductances, and the Python-based pre-design tool allowed for accurate and fast estimation of required turns based on frequency and core data. The COMSOL models allowed for accurate simulations that were used to compare and optimise the measured values. Team collaboration and communication with supervisors was consistent and productive throughout.

However, the project also encountered several critical limitations. The initial literature review lacked sufficient depth, particularly around foundational topics such as B-H curves, which later proved important for understanding core saturation. Measurement consistency was a recurring issue. The VNA setup was prone to unreliable connections, and skipping VNA calibration led to data that was more in-line with predictions than with VNA calibration. This raised concerns about the accuracy of capacitance and resistance extractions. The team, however, was quickly able to find an alternative method to measure DC resistances in the coils. AC resistance measurements were attempted both via the VNA and oscilloscope, but neither method yielded reliable results, largely due to low signal levels and the difficulty of isolating phasor components.

Time management was a substantial challenge. Although core losses and thermal behaviour were identified as key thesis themes, limited time meant these aspects were not investigated beyond preliminary estimations. The use of COMSOL was delayed until the final design phase due to inexperience with the tool, which led to only simulating parasitic capacitances and inductances. Other features of COMSOL could have been utilised think of thermal simulations and resistance calculations. LTspice simulations were similarly underutilised; most time was spent troubleshooting measurement inconsistencies rather than modelling idealised transformer behaviour. Moreover, for each transformer configuration, only one prototype was built, which significantly limited the ability to assess experimental variability or draw statistically meaningful conclusions. Inconsistency also affected data organisation: a single, unstructured spreadsheet served as the main repository, which eventually became difficult to navigate and

analyse systematically.

For future work, several improvements are clear. First, the project scope should be narrowed to reduce variables and improve consistency. Although the study focused solely on toroidal cores, each core size came with a different material and permeability, which complicated direct comparisons. Future studies should isolate either geometry or material while holding the other constant. Secondly, more samples per configuration should be built and tested to increase the validity of comparative results. Third, core shape alternatives (such as E-cores or planar geometries) should be explored to assess the generality of conclusions drawn about toroidal performance. On the modelling side, LTspice simulations should be employed earlier and more systematically - not only for validation, but as a design exploration tool. Similarly, more structured use of COMSOL could support a better understanding of parasitic effects, field distributions, and thermal behaviour. Finally, improving data management protocols, either in the form of structured logging or standardised templates, would significantly reduce friction during analysis and increase traceability of results.

Overall, while the project successfully demonstrated the feasibility of using the IEEE Std 390 in high-frequency transformer modelling and validated several analytical predictions, it also highlighted the challenges of maintaining consistency, accuracy, and scope control in a compressed development cycle.

9

Conclusion

The thesis project set out to evaluate whether a high-frequency transformer operating in the 1-3MHz range could be modelled using the IEEE Std 390 equivalent circuit model. By combining analytical, numerical and empirical modelling techniques, the project addressed a gap in modelling standards at high frequencies. To an extent, the project succeeded.

A literature study was first conducted to get a basic grasp on transformer operation, after which a programme of requirements and set of SMART goals were drafted. Multiple transformer prototypes were designed and constructed. By first using the Bode 100 VNA to obtain inductance, resistance and parasitic capacitance values, a model was built in LTSpice based on the IEEE 390 equivalent circuit. This model proved to work quite reliably and could produce plots close to what was measured in reality. Additionally, comparisons between measured and analytical calculations showed that values matched within 10% for *most* prototypes. The saturation voltages and resistance deviated the most, with errors around 30%. This is believed to be due to structural inaccuracies and faulty measurements. The absolute average errors can be found in table 9.1, accounting for outliers.

Measurement	Average absolute percentage error
L_1	3.96
L_2	3.63
R_{DC}	11.54
C_{12}	98.91
V_{sat}	19.93

Table 9.1: Average absolute error of each measurement

Simultaneously, a model in COMSOL was built to validate the VNA measurements. This proved to be quite useful as values such as parasitic capacitances could not be found analytically. After all the measurements were taken, trends were spotted and discussed. The trends also helped in understanding the different core configurations and in building an intuition on transformer behaviour. Final prototyping followed.

The final design met most of the key requirements: the transformer successfully converted an AC signal, operated at above 1MHz without saturating and maintained above 80% efficiency. The transformer and driving circuit fit within the 8x8x5cm constraint, confirming feasibility for compact electronics applications. Operating at 2A, 50V proved to be harder, and had not been completely tested. The Tiny core was not suitable as it would saturate below 2A. The medium and the large core were found to be suitable, saturating near or above 2A.

The SMART goals as set in chapter 2 were mostly met. *Specific*: the IEEE 390 circuit equivalent model was tested in LTSpice and applied only to TL 20. It was not used for validating the final prototype. This was due to mismanagement of time and planning mistakes. *Measurable*: The 10% deviation limit

was not attained throughout all measurements and calculations. This is due to a few reasons: faulty measurements and VNA sensitivity; 19.93% average errors in the saturation voltage as a result of structural inaccuracies; capacitances varied heavily depending on core material and even core presence. *Assignable*: The subgroup was able to work efficiently and all progress and findings were documented in an acceptable manner. *Realistic*: COMSOL was integrated only at critical stages of the project as a means of validation, avoiding reliance on 3D simulations for each step. *Time-related*: All builds were completed in the 8 weeks, however management of time and resources could have been better so analysis could be more thorough, especially regarding the IEEE 390 LTSpice simulations.

Ultimately, the project succeeded in designing, modelling, and characterising multiple transformer prototypes, culminating in a validated medium-core, 5-turn litz-wire design. This lays the groundwork for future exploration of core geometries beyond toroids.

References

[1] "IEEE Standard for Pulse Transformers". In: *ANSI/IEEE Std 390-1987* (1987), pp. 1–32. DOI: 10.1109/IEEESTD.1987.79640.

[2] Erick I. Pool-Mazun et al. "An Integrated Solid-State Transformer With High-Frequency Isolation for EV Fast-Charging Applications". In: *IEEE Journal of Emerging and Selected Topics in Industrial Electronics* 1.1 (2020), pp. 46–56. DOI: 10.1109/JESTIE.2020.3003355.

[3] Weichong Yao et al. "Integration of SIC devices and high-frequency transformer for high-power renewable energy applications". In: *Energies* 16.3 (Feb. 2023), p. 1538. DOI: 10.3390/en16031538.

[4] P. Seshasai Kumar. "Design of high frequency power transformer for switched mode power supplies". In: *2016 International Conference on Emerging Trends in Engineering, Technology and Science (ICETETS)*. 2016, pp. 1–5. DOI: 10.1109/ICETETS.2016.7603076.

[5] Joydeb Das et al. "Design and Analysis of Soft Switching PWM DC-DC Power Converter with High-Frequency Transformer Link for Portable Arc Welding Machine". In: *2020 IEEE Region 10 Symposium (TENSYMP)*. 2020, pp. 1820–1823. DOI: 10.1109/TENSYMP50017.2020.9230803.

[6] Juncheng Li et al. "High-frequency Modulated Transformer for Multi-Contrast MRI Super-Resolution". In: *IEEE Transactions on Medical Imaging* (2025), pp. 1–1. DOI: 10.1109/TMI.2025.3558164.

[7] Pradeep Vishnuram et al. "A comprehensive overview of power converter topologies for induction heating applications". In: *International Transactions on Electrical Energy Systems* 30.10 (Aug. 2020). DOI: 10.1002/2050-7038.12554.

[8] Robert W Erickson and Dragan Maksimović. *Fundamentals of Power Electronics*. 3rd ed. Springer Charm, 2020.

[9] M. K. Kazimierczuk. *High-frequency magnetic components*. 2nd ed. Chichester, West Sussex: Wiley Blackwell, 2014.

[10] Shaokang Luan and Hongbo Zhao. "Parasitic Capacitances in Magnetic Components: Overview and Perspectives". In: *IEEE Open Journal of Power Electronics* PP (Jan. 2025), pp. 1–18. DOI: 10.1109/OJPEL.2025.3540079.

[11] Y. Zhang et al. "Comprehensive Analysis of Switching Transient Mechanisms in SiC MOSFETs With Different Parasitic Elements". In: *IEEE Transactions on Power Electronics* 34.3 (Mar. 2019), pp. 2527–2543. DOI: 10.1109/TPEL.2018.2847333.

[12] "IEEE Standard for Pulse Transformers". In: *ANSI/IEEE Std 390-1987* (1987), pp. 1–32. DOI: 10.1109/IEEESTD.1987.79640.

[13] J. Biernacki and D. Czarkowski. "High frequency transformer modeling". In: *ISCAS 2001. The 2001 IEEE International Symposium on Circuits and Systems (Cat. No.01CH37196)*. Vol. 3. 2001, 676–679 vol. 2. DOI: 10.1109/ISCAS.2001.921401.

[14] Abdallah Chanane, Hamza Houassine, and Ouahid Bouchhida. "Enhanced modelling of the transformer winding high frequency parameters identification from measured frequency response analysis". In: *IET Generation, Transmission &; Distribution* 13.8 (Mar. 2019), pp. 1339–1345. DOI: 10.1049/iet-gtd.2018.5514.

[15] Ahmed Abu-Siada et al. "Estimating Power Transformer High Frequency model parameters using frequency response analysis". In: *IEEE Transactions on Power Delivery* 35.3 (June 2020), pp. 1267–1277. DOI: 10.1109/tpwrd.2019.2938020.

[16] J. W. Kolar et al. "EMI Issues in High-Frequency Power Electronic Converters". In: *IEEE Transactions on Industrial Electronics* 55.9 (2007), pp. 3006–3015. DOI: 10.1109/TIE.2007.893061.

[17] P. L. Dowell. “Effects of Eddy Currents in Transformer Windings”. In: *Proceedings of the IEE* 113.8 (1966), pp. 1387–1394. DOI: 10.1049/pi.1966.0213.

[18] E. Sanchez et al. “3D FEA-Based Optimization of High-Frequency Transformers in Resonant Converters”. In: *IEEE Transactions on Magnetics* 50.2 (2014), pp. 845–848. DOI: 10.1109/TMAG.2013.2284172.

[19] European Alternative Fuels Observatory. *The Netherlands in 2024: Almost 35% market share for bevs, fleet surpasses 6%*. Jan. 2025. URL: https://alternative-fuels-observatory.ec.europa.eu/general-information/news/netherlands-2024-almost-35-market-share-bevs-fleet-surpasses-6.

[20] Fawwaz T. Ulaby, Eric Michielssen, and Umberto Ravaioli. *Fundamentals of Applied Electromagnetics, Global Edition*. Mar. 2015.

[21] Richard M. Bozorth. *Ferromagnetism*. Jan. 1978.

[22] Ferroxcube. *Material specification 3E6*. Tech. rep. Sept. 2008. URL: https://elnamagnetics.com/wp-content/uploads/library/Ferroxcube-Materials/3E6_Material_Specification.pdf.

[23] Designed by Akacia System www.akacia.com.tw. *Products-Ferroxcube*. URL: https://www.ferroxcube.com/en-global/products_ferroxcube/detail/toroid/epoxy_coated_toroid.

[24] Designed by Akacia System www.akacia.com.tw. *Products-Ferroxcube*. URL: https://www.ferroxcube.com/en-global/products_ferroxcube/detail/shape_cores_accessories/p_cores.

[25] Designed by Akacia System www.akacia.com.tw. *Products-Ferroxcube*. URL: https://www.ferroxcube.com/en-global/products_ferroxcube/detail/shape_cores_accessories/rm_cores.

[26] Designed by Akacia System www.akacia.com.tw. *Products-Ferroxcube*. URL: https://www.ferroxcube.com/en-global/products_ferroxcube/detail/shape_cores_accessories/e_cores.

[27] Designed by Akacia System www.akacia.com.tw. *Products-Ferroxcube*. URL: https://www.ferroxcube.com/en-global/products_ferroxcube/detail/shape_cores_accessories/er_and_etd_cores.

[28] Designed by Akacia System www.akacia.com.tw. *Products-Ferroxcube*. URL: https://www.ferroxcube.com/en-global/products_ferroxcube/detail/shape_cores_accessories/ec_cores.

[29] Designed by Akacia System www.akacia.com.tw. *Products-Ferroxcube*. URL: https://www.ferroxcube.com/en-global/products_ferroxcube/detail/shape_cores_accessories/pq_cores.

[30] Designed by Akacia System www.akacia.com.tw. *Products-Ferroxcube*. URL: https://www.ferroxcube.com/en-global/products_ferroxcube/detail/shape_cores_accessories/ep_and_epx_cores.

[31] Zenong Li et al. “A Review of Magnetic Core Materials, Core Loss Modeling and Measurements in High-Power High-Frequency Transformers”. In: *CPSS Transactions on Power Electronics and Applications* 7.4 (2022), pp. 359–373. DOI: 10.24295/CPSSTPEA.2022.00033.

[32] F. Fiorillo et al. “Soft magnetic materials”. In: *Wiley Encyclopedia of Electrical and Electronics Engineering* (Dec. 1999). DOI: 10.1002/047134608x.w4504. URL: https://doi.org/10.1002/047134608x.w4504.

[33] Muhammad Kamal Ahmad et al. “Comparison and analysis of core materials for high frequency (1MHz) planar transformers”. In: *2018 International Conference on Computing, Mathematics and Engineering Technologies (iCoMET)* (Mar. 2018). DOI: 10.1109/icomet.2018.8346429. URL: https://doi.org/10.1109/icomet.2018.8346429.

[34] Haiwang Li et al. “Integrated MEMS toroidal transformer with Ni-ZN ferrite core for power supply on chip”. In: *IEEE Transactions on Power Electronics* 37.9 (Mar. 2022), pp. 10075–10080. DOI: 10.1109/tpel.2022.3160698. URL: https://doi.org/10.1109/tpel.2022.3160698.

[35] Pengning Zhang et al. “Research on multi-objective optimization method in the design of high-power nanocrystalline alloy high-frequency transformer”. In: *Journal of Magnetism and Magnetic Materials* 606 (July 2024), p. 172389. DOI: 10.1016/j.jmmm.2024.172389. URL: https://doi.org/10.1016/j.jmmm.2024.172389.

[36] Jorge Ortíz-Marín et al. “Design and implementation of a Central-Tapped Medium Frequency Transformer with nanocrystalline core for high-efficiency DC-DC SAB converters”. In: *Electric Power Systems Research* 227 (Nov. 2023), p. 109900. DOI: 10.1016/j.epsr.2023.109900. URL: https://doi.org/10.1016/j.epsr.2023.109900.

[37] Gijs Lagerweij and Mohamad Ghaffarian Niasar. “Design of a high□frequency transformer based on amorphous cut cores for insulation breakdown testing”. In: *High Voltage* 9.5 (June 2024), pp. 1183–1194. DOI: 10.1049/hve2.12460. URL: https://doi.org/10.1049/hve2.12460.

[38] OMICRON Lab. *Bode 100 - Application Note*. Tech. rep. 2017. URL: https://picotest.com/wp-content/uploads/2024/03/Bode-100-User-Manual-ENU10060502.pdf.

[39] Daniela Rodriguez-Sotelo et al. “Power Losses Models for magnetic Cores: A review”. In: *Micromachines* 13.3 (Mar. 2022), p. 418. DOI: 10.3390/mi13030418. URL: https://pmc.ncbi.nlm.nih.gov/articles/PMC8954854/.

[40] *3E65 Material Specification*. FXC10000012. Ferroxcube. Mar. 2022. URL: https://www.ferroxcube.com/de-DE/download/download/108.

[41] *Toroid 14/9/5 Product Specification*. Ferroxcube. 2016. URL: https://www.ferroxcube.com/upload/media/product/file/Pr_ds/T_14_9_5.pdf.

[42] *3E10/3E12 Material Specification*. FXC10000012. Ferroxcube. Mar. 2022. URL: https://www.ferroxcube.com/de-DE/download/download/208.

[43] *Toroid 29/19/7.6 Product Specification*. Ferroxcube. 2016. URL: https://www.ferroxcube.com/upload/media/product/file/Pr_ds/T_29_19_7.6.pdf.

[44] *3C94 Material Specification*. Ferroxcube. Sept. 2008. URL: https://ferroxcube.home.pl/prod/assets/3c94.pdf.

[45] *Toroid 36/23/15 Product Specification*. Ferroxcube. 2016. URL: https://www.ferroxcube.com/upload/media/product/file/Pr_ds/T_36_23_15.pdf.

[46] Ravi Kumar Kaparapu. “Design and Implementation of a Pulse Transformer and Study on Ageing of Oil Impregnated Paper under Pulsed Stresses”. MA thesis. Delft University of Technology, Aug. 2022. URL: https://repository.tudelft.nl/record/uuid:9f1ee452-0e88-4bc7-8179-a246fe705af4.

[47] H.A. Wheeler. “Formulas for the skin effect”. In: *Proceedings of the IRE* 30.9 (Sept. 1942), pp. 412–424. DOI: 10.1109/jrproc.1942.232015. URL: https://doi.org/10.1109/jrproc.1942.232015.

[48] COMSOL Multiphysics. *An Introduction to the Theory of Electrostatics*. 2019. URL: https://www.comsol.com/multiphysics/electrostatics-theory.

[49] *15. Coupled coils — EE2E11 Electrical energy conversion*. URL: https://jianning.info/course/ee2e11/reader/coupled_coil.html.

A

Code

A.1. Pre-design Python script for number of turns

```python
import csv

def mm2_to_m2(mm2):
    return mm2 * 1e-6

def mt_to_t(mT):
    return mT * 1e-3

def calculate_turns(E_rms, B_T, A_m2, freq):
    return E_rms / (4.44 * freq * B_T * A_m2)

def main():
    # Input parsing
    A_list_input = input("Enter cross-sectional areas in mm² (comma-separated): ")
    A_list_mm2 = [float(a.strip()) for a in A_list_input.split(',')]
    A_list_m2 = [mm2_to_m2(a) for a in A_list_mm2]

    B_input_mT = float(input("Enter maximum flux density B_max in millitesla (mT): "))
    B_max = mt_to_t(B_input_mT)

    E_rms = float(input("Enter RMS voltage E in volts (V): "))

    # Frequency list
    freq_list = [10_000, 50_000] + \
                list(range(100_000, 1_100_000, 100_000)) + \
                list(range(1_200_000, 2_200_000, 200_000)) + [3_000_000]

    # Prepare CSV output
    csv_filename = "transformer_turns_output.csv"
    with open(csv_filename, mode='w', newline='') as file:
        writer = csv.writer(file)
        writer.writerow(["Area (mm²)", "Frequency (kHz)", "Turns (N)", "Warning"])

        print("\nResults (Number of Turns N):")
        for i, A in enumerate(A_list_m2):
            area_mm2 = A_list_mm2[i]
            print(f"\n--- For Area: {area_mm2:.1f} mm² ---")
            for f in freq_list:
                N = calculate_turns(E_rms, B_max, A, f)
                freq_khz = f / 1000
                warning = ""
                if N < 1:
                    warning = "<-- WARNING: N < 1"
                    print(f"f = {freq_khz:.1f} kHz: N = {N:.2f} {warning}")
                else:
                    print(f"f = {freq_khz:.1f} kHz: N = {N:.2f}")
                writer.writerow([area_mm2, freq_khz, round(N, 2), warning])
```

```
48
49      print(f"\nCSV␣file␣saved␣as:␣{csv_filename}")
50
51  if __name__ == "__main__":
52      main()
```

A.2. Oscilloscope CSV to Graph Python Script

```
1  import pandas as pd
2  import numpy as np
3  import matplotlib.pyplot as plt
4
5  # Load CSV files
6  file1 = "osso␣scope␣core␣satu\ALL0000\F0000CH1.CSV"
7  file2 = "osso␣scope␣core␣satu\ALL0000\F0000CH2.CSV"
8
9  # Read files and skip first two rows of metadata
10 df1 = pd.read_csv(file1, skiprows=2)
11 df2 = pd.read_csv(file2, skiprows=2)
12
13 data1 = df1.iloc[:, [3, 4]].dropna().astype(float)
14 data2 = df2.iloc[:, [3, 4]].dropna().astype(float)
15 data1.columns = ['Time', 'Voltage␣(CH1)']
16 data2.columns = ['Time', 'Voltage␣(CH2)']
17
18 # Normalise time to start from 0
19 data1['Time'] -= data1['Time'].iloc[0]
20 data2['Time'] -= data2['Time'].iloc[0]
21
22 # Compute Vrms and Vpp
23 vrms1 = np.sqrt(np.mean(data1['Voltage␣(CH1)'] ** 2))
24 vpp1 = data1['Voltage␣(CH1)'].max() - data1['Voltage␣(CH1)'].min()
25
26 vrms2 = np.sqrt(np.mean(data2['Voltage␣(CH2)'] ** 2))
27 vpp2 = data2['Voltage␣(CH2)'].max() - data2['Voltage␣(CH2)'].min()
28
29 # Plotting
30 plt.figure(figsize=(12, 6))
31 plt.plot(data1['Time']*1000, data1['Voltage␣(CH1)'], label=f'Inductor␣(Vrms={vrms1:.2f}␣V,␣
       Vpp={vpp1:.2f}␣V)')
32 plt.plot(data2['Time']*1000, data2['Voltage␣(CH2)'], label=f'Resistor␣(Vrms={vrms2:.2f}␣V,␣
       Vpp={vpp2:.2f}␣V)')
33 plt.title('TL␣5␣Turns:␣Voltage␣vs␣Time')
34 plt.xlabel('Time␣(ms)')
35 plt.ylabel('Voltage␣(V)')
36 plt.grid(True)
37
38 # Increase y-axis ticks
39 plt.locator_params(axis='y', nbins=20)
40
41 plt.legend(loc="upper␣right")
42 plt.tight_layout()
43 plt.show()
```

B

Frequency Response Graphs from VNA

B.1. Tiny Toroid 1 Turn Gain, Config. 1

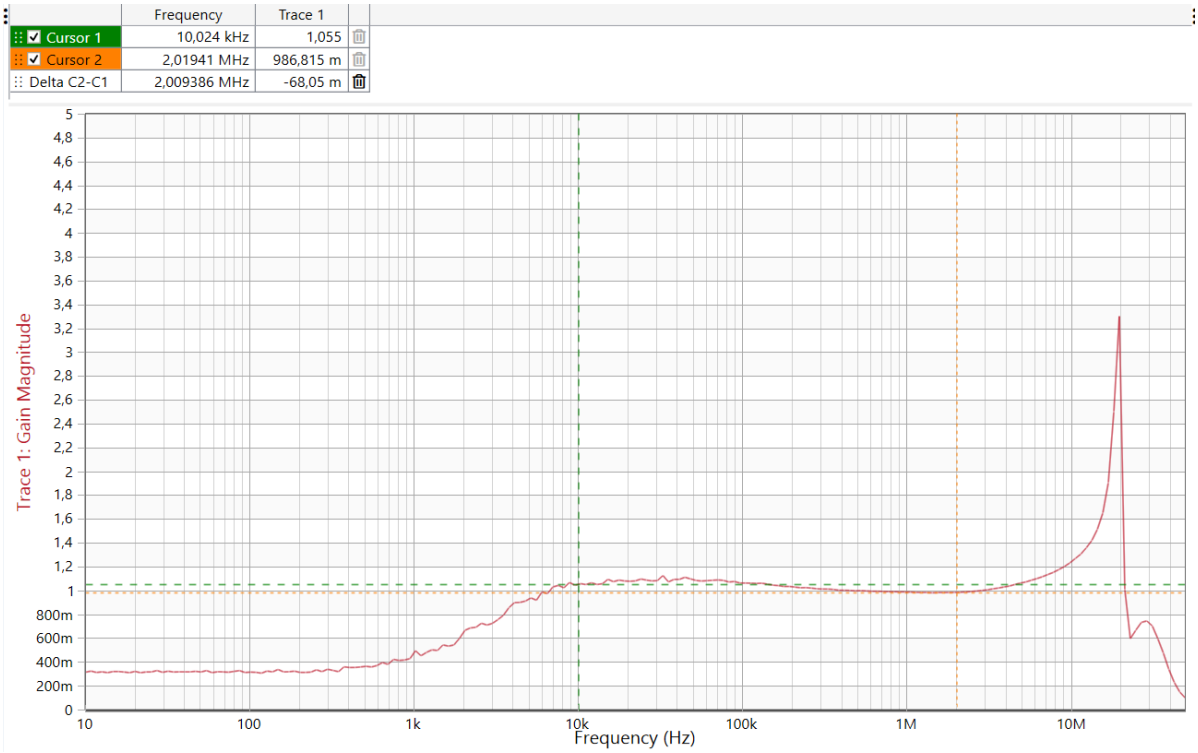

Figure B.1: Gain plot of Tiny Toroid with 1 turn

B.2. Tiny Toroid 3 Turns Gain, Config. 1

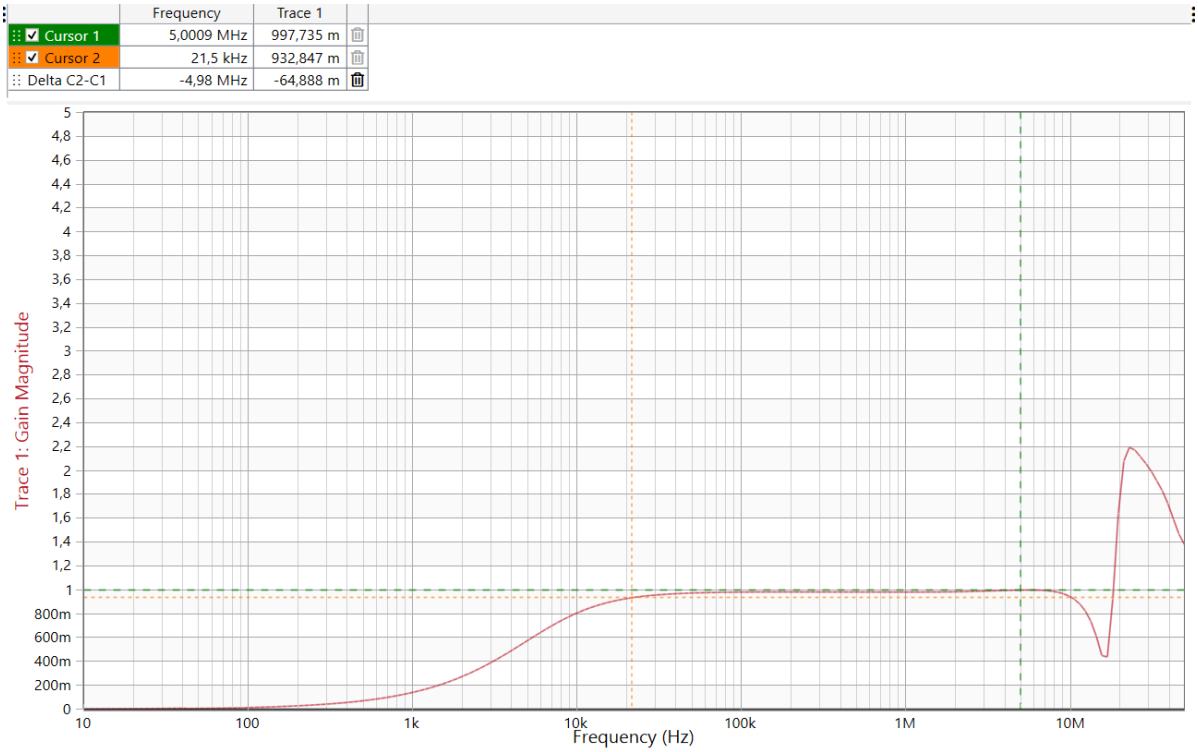

Figure B.2: Gain plot of Tiny Toroid with 3 turns

B.3. Medium Toroid 5 Turns Gain, Config. 1

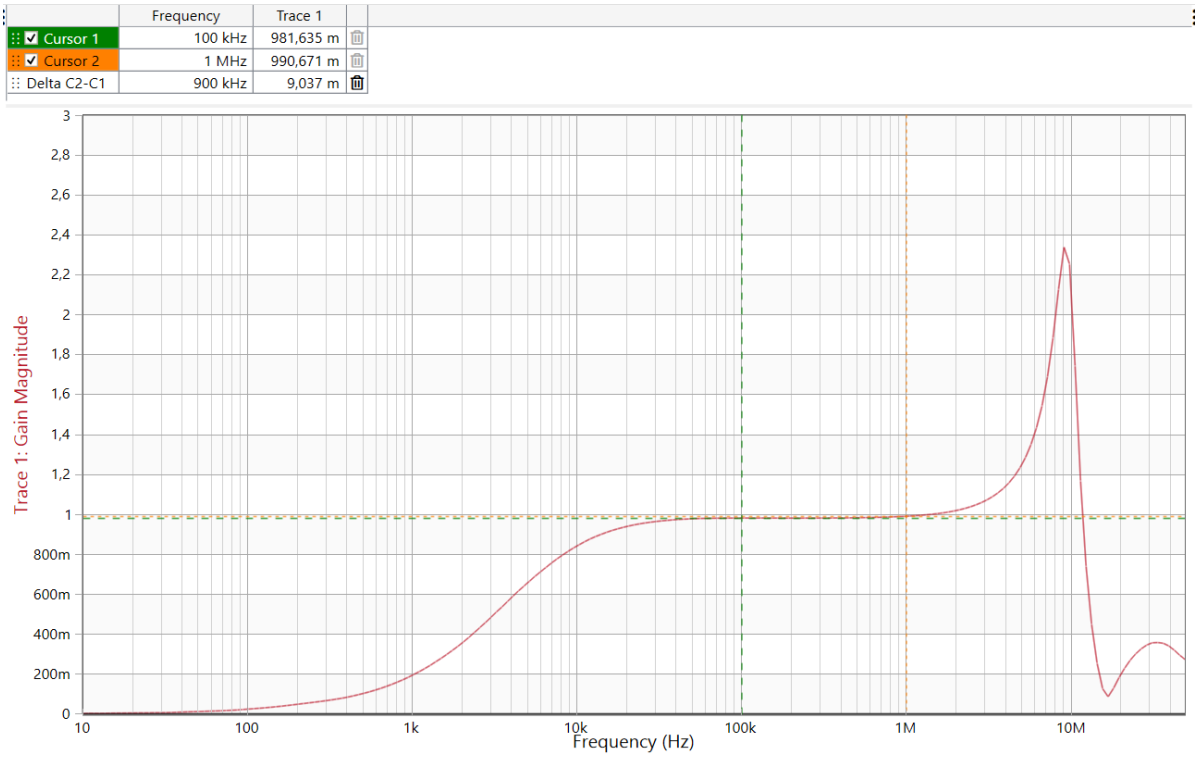

Figure B.3: Gain plot of Medium Toroid with 5 turns

B.4. Medium Toroid 10 Turns Gain, Config. 1

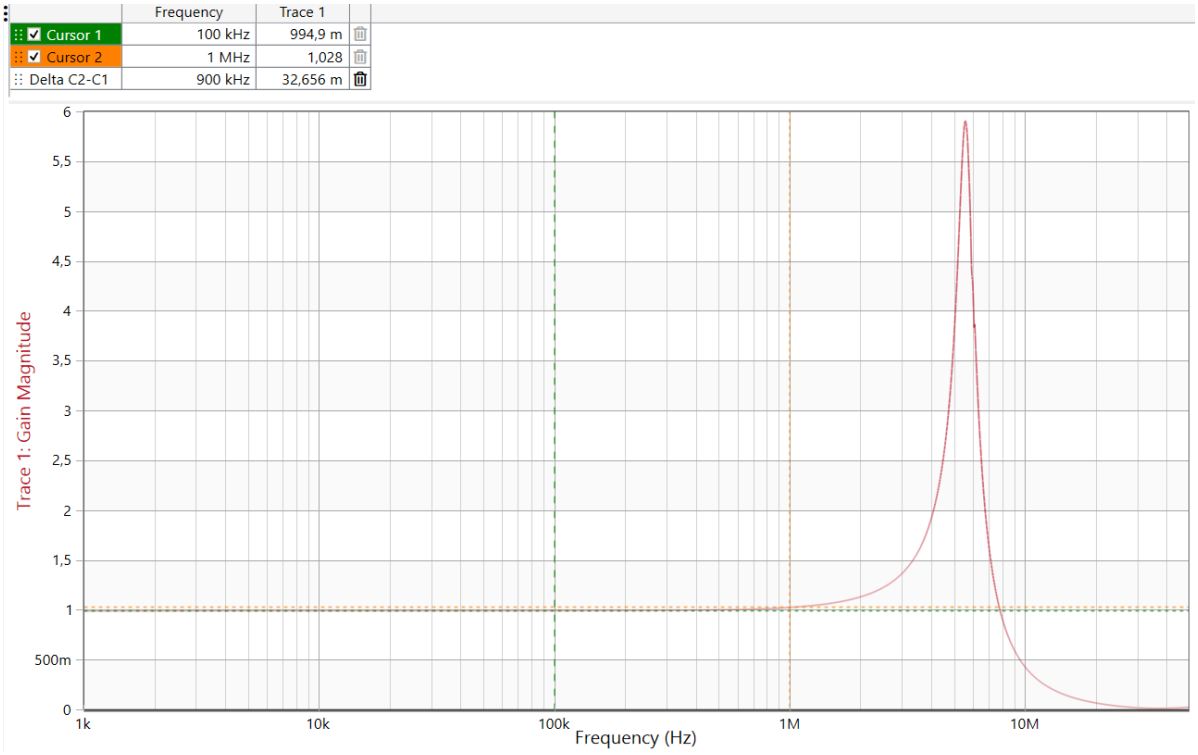

Figure B.4: Gain plot of Medium Toroid with 10 turns

B.5. Medium Toroid 5 Turns Gain, Config. 2

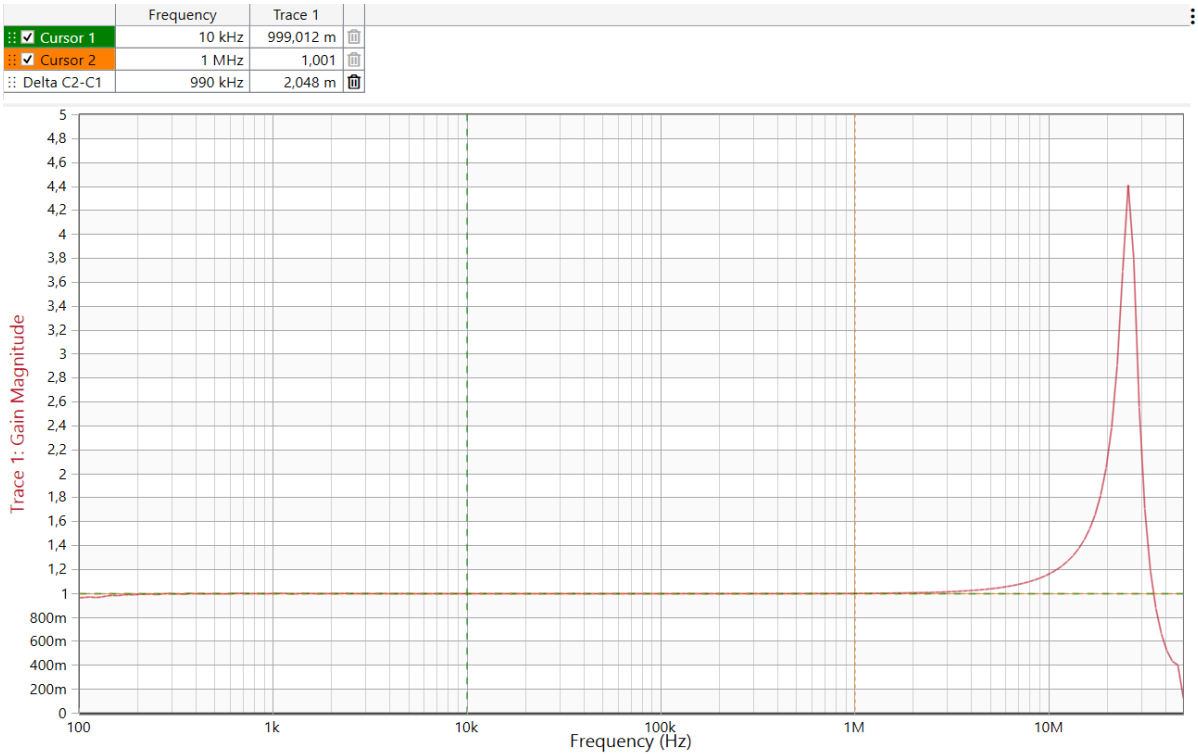

Figure B.5: Gain plot of Medium Toroid with 5 turns in configuration 2

B.6. Large Toroid 20 Turns Gain, Config. 1

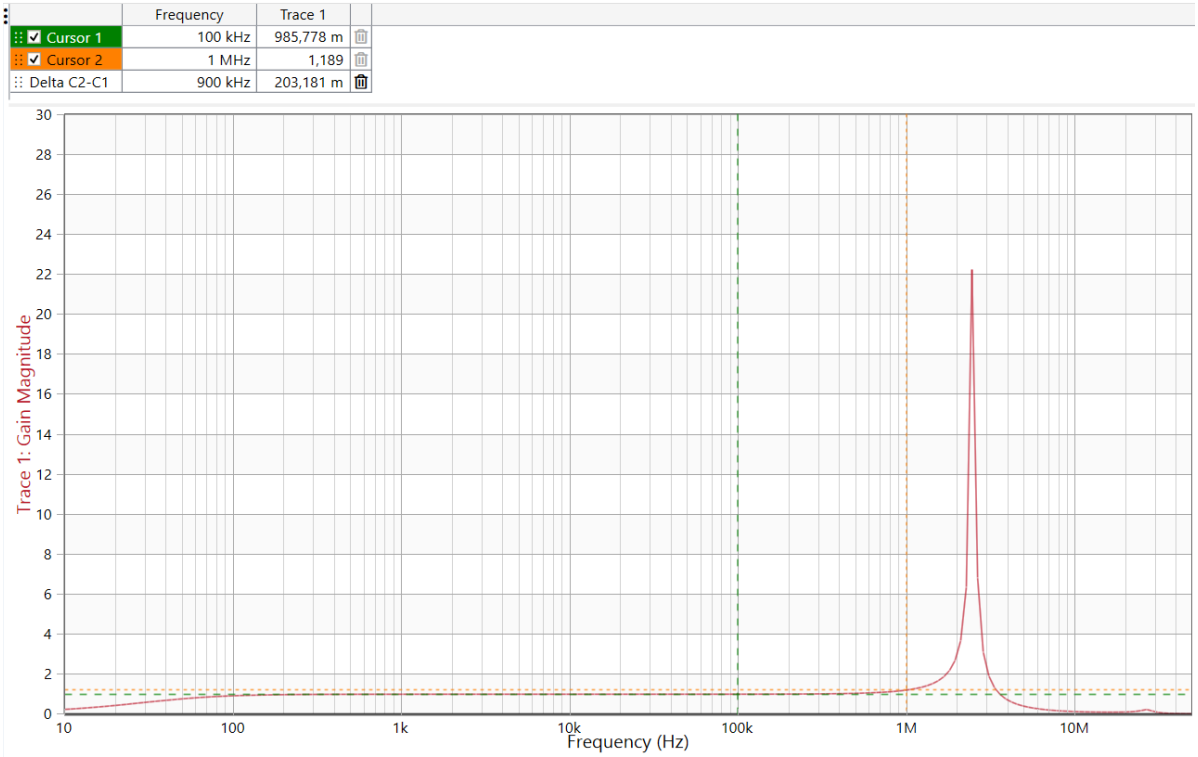

Figure B.6: Gain plot of Large Toroid with 20 turns

B.7. Large Toroid 13 Turns Gain, Config. 2

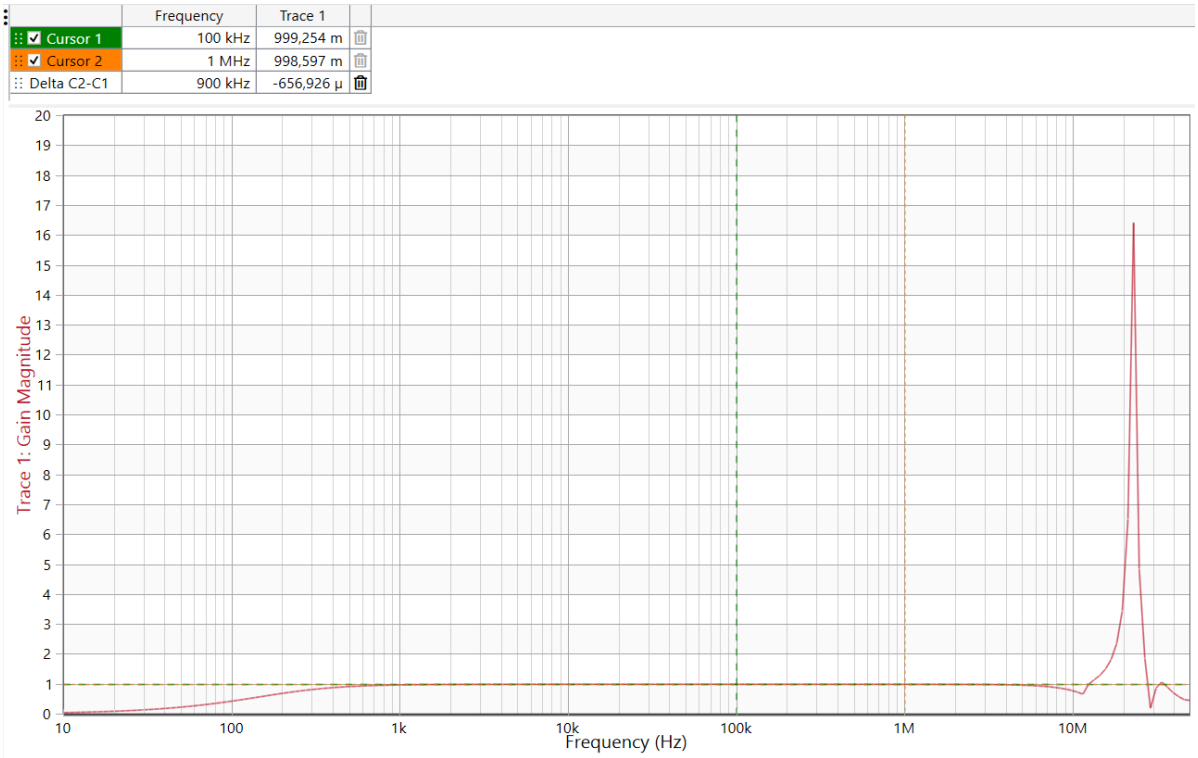

Figure B.7: Gain plot of Large Toroid with 13 turns in configuration 2

C

Primary Side Inductance Graphs from VNA

C.1. Tiny Toroid 1 Turn Primary Inductance, Config. 1

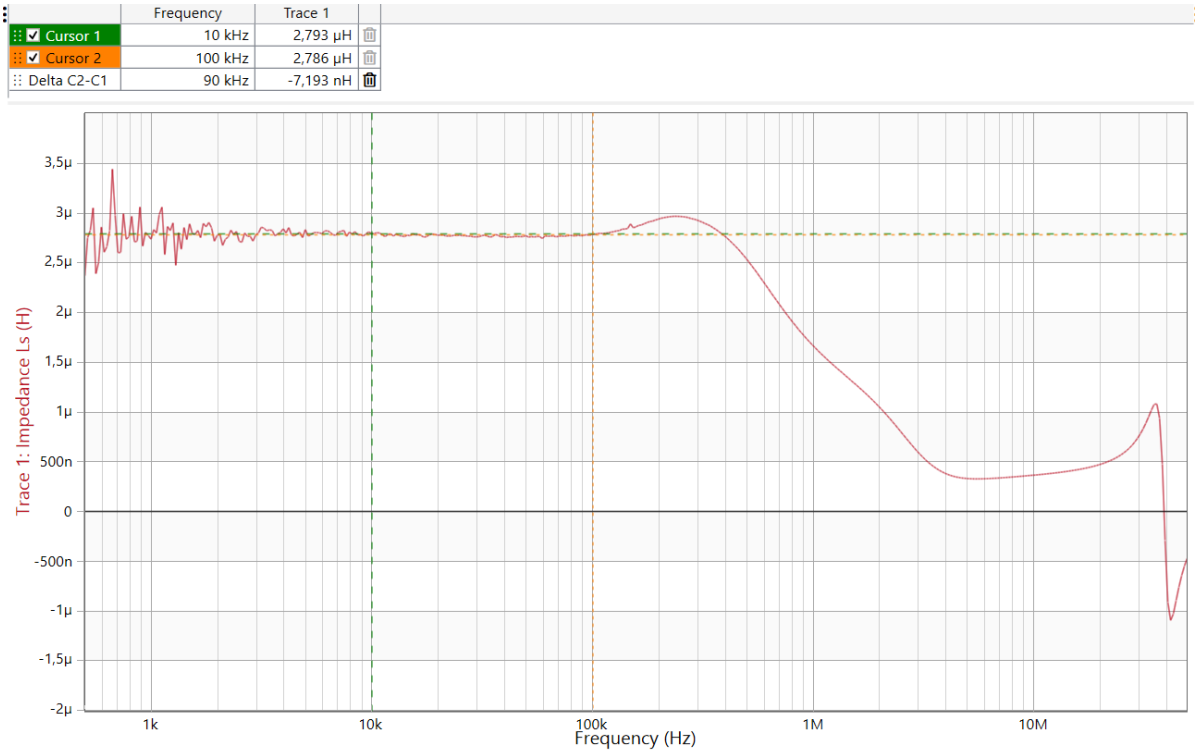

Figure C.1: Inductance plot of Tiny Toroid with 1 turn

C.2. Tiny Toroid 2 Turns Primary Inductance, Config. 1

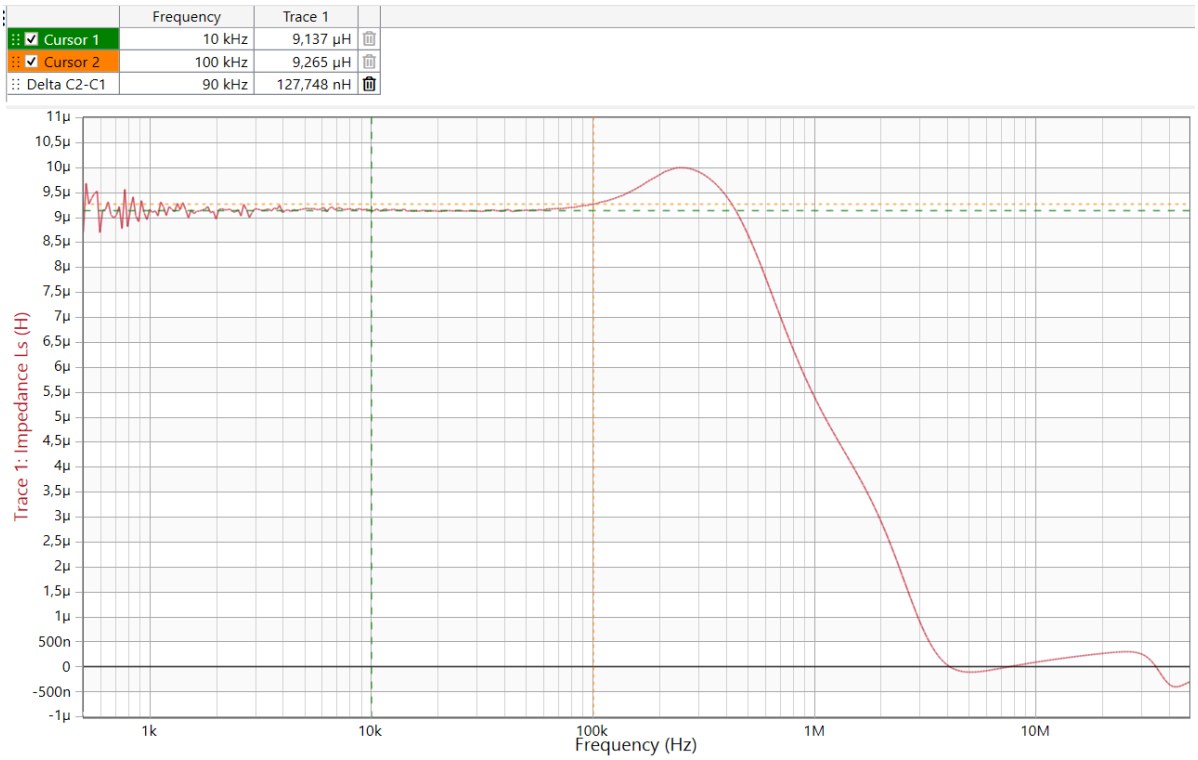

Figure C.2: Inductance plot of Tiny Toroid with 2 turns

C.3. Tiny Toroid 3 Turns Primary Inductance, Config. 1

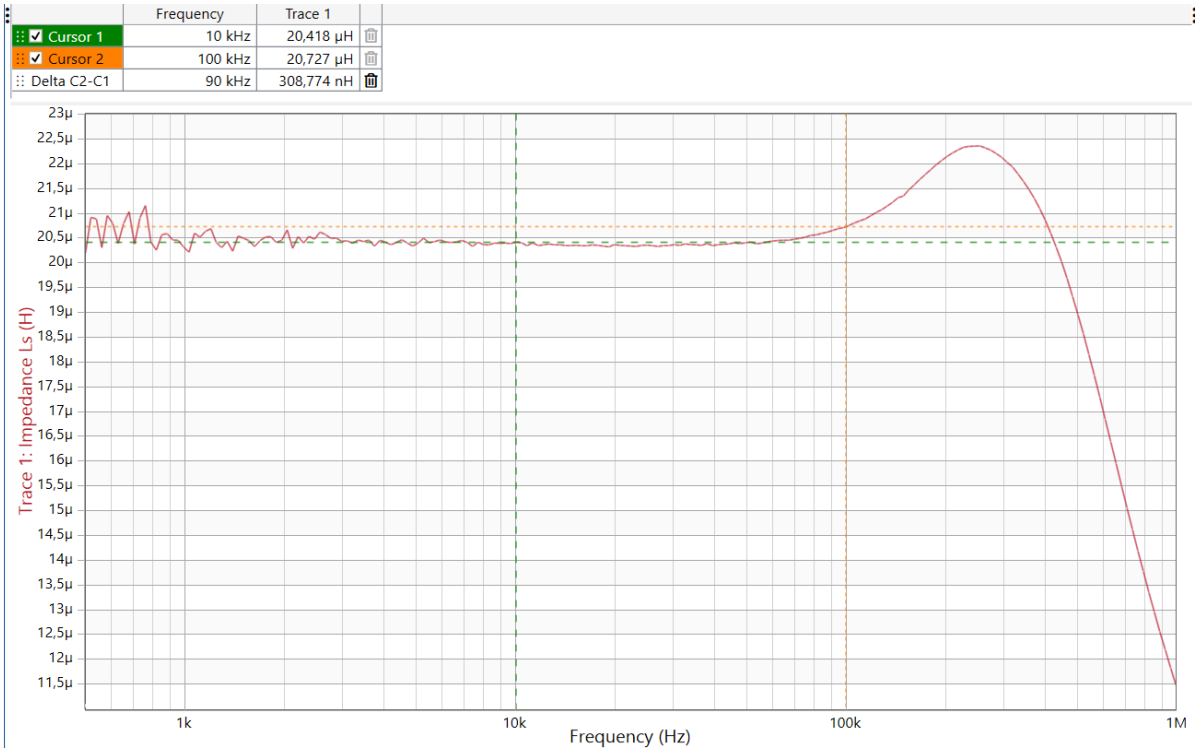

Figure C.3: Inductance plot of Tiny Toroid with 3 turns

C.4. Tiny Toroid 3 Turns Primary Inductance, Braided

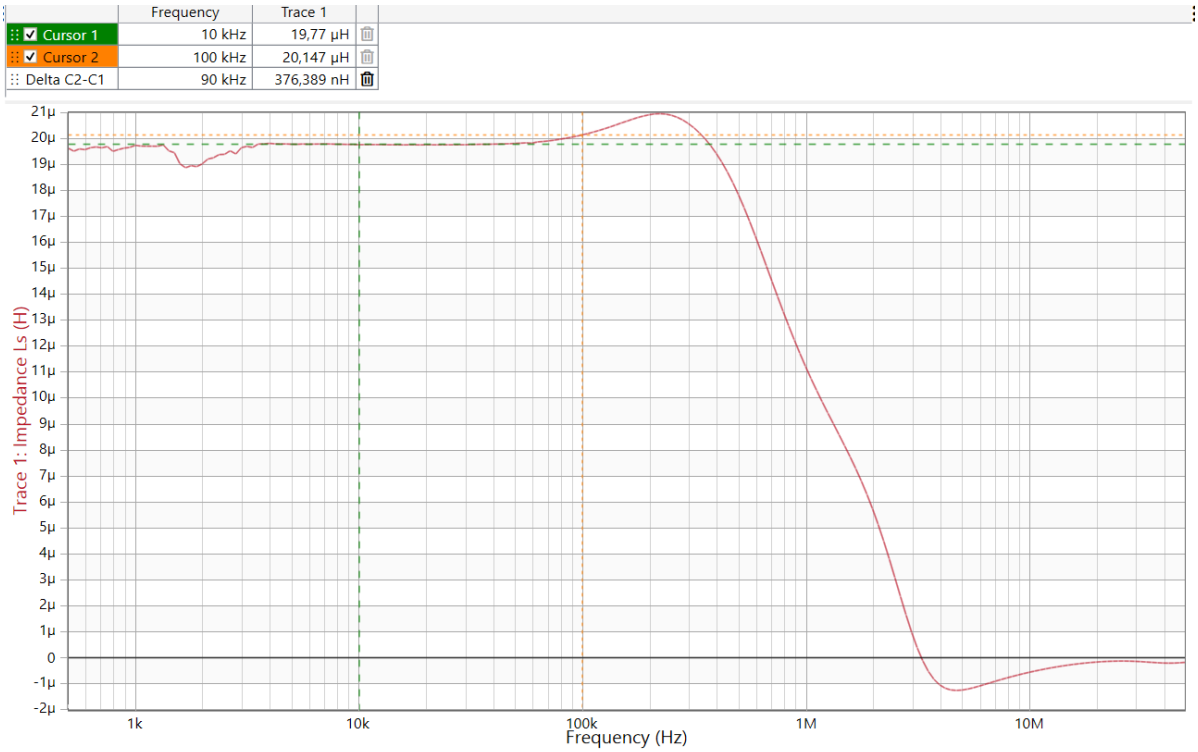

Figure C.4: Inductance plot of Tiny Toroid with 3 turns braided

C.5. Medium Toroid 5 Turns Primary Inductance, Config. 1

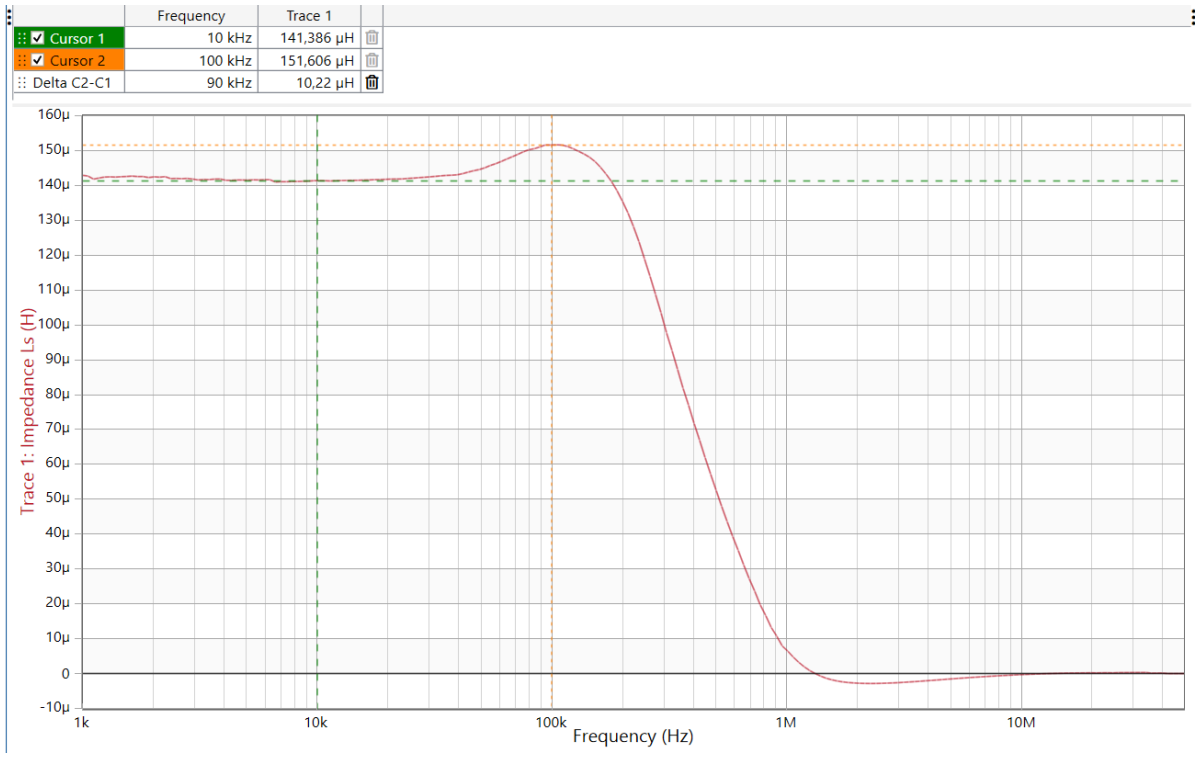

Figure C.5: Inductance plot of Medium Toroid with 5 turns

C.6. Medium Toroid 10 Turns Primary Inductance, Config. 1

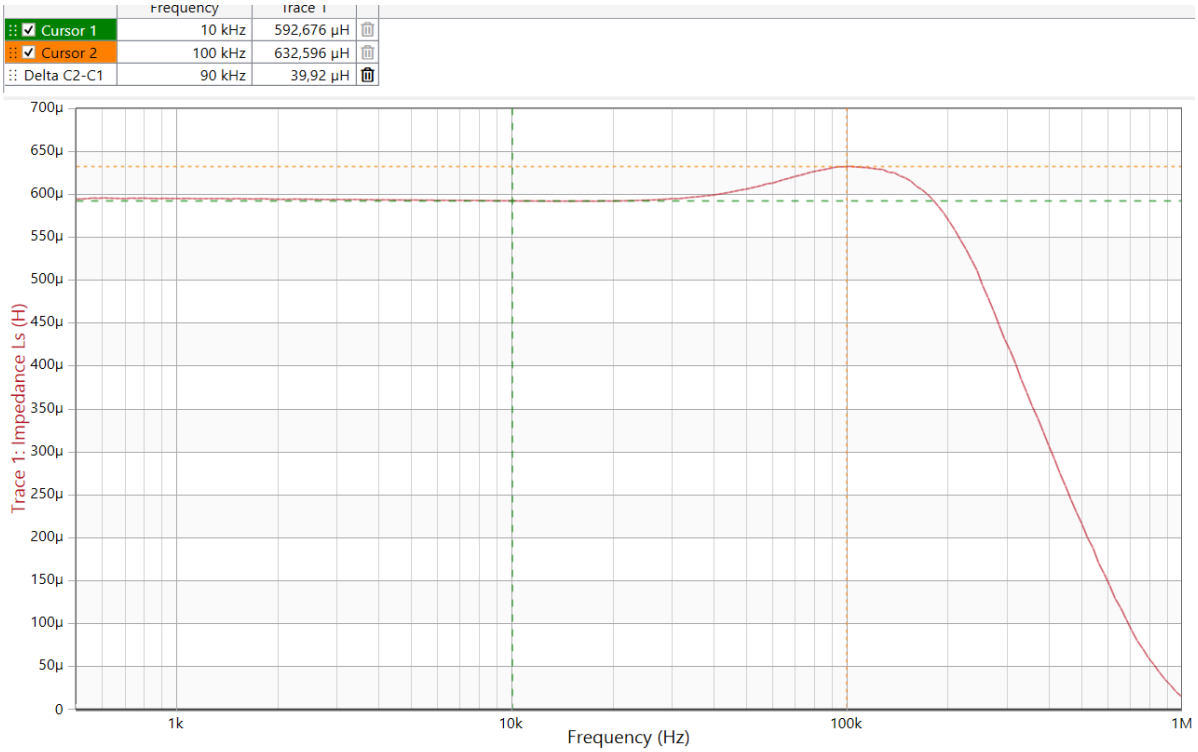

Figure C.6: Inductance plot of Medium Toroid with 10 turns

C.7. Medium Toroid 5 Turns Primary Inductance, Config. 2

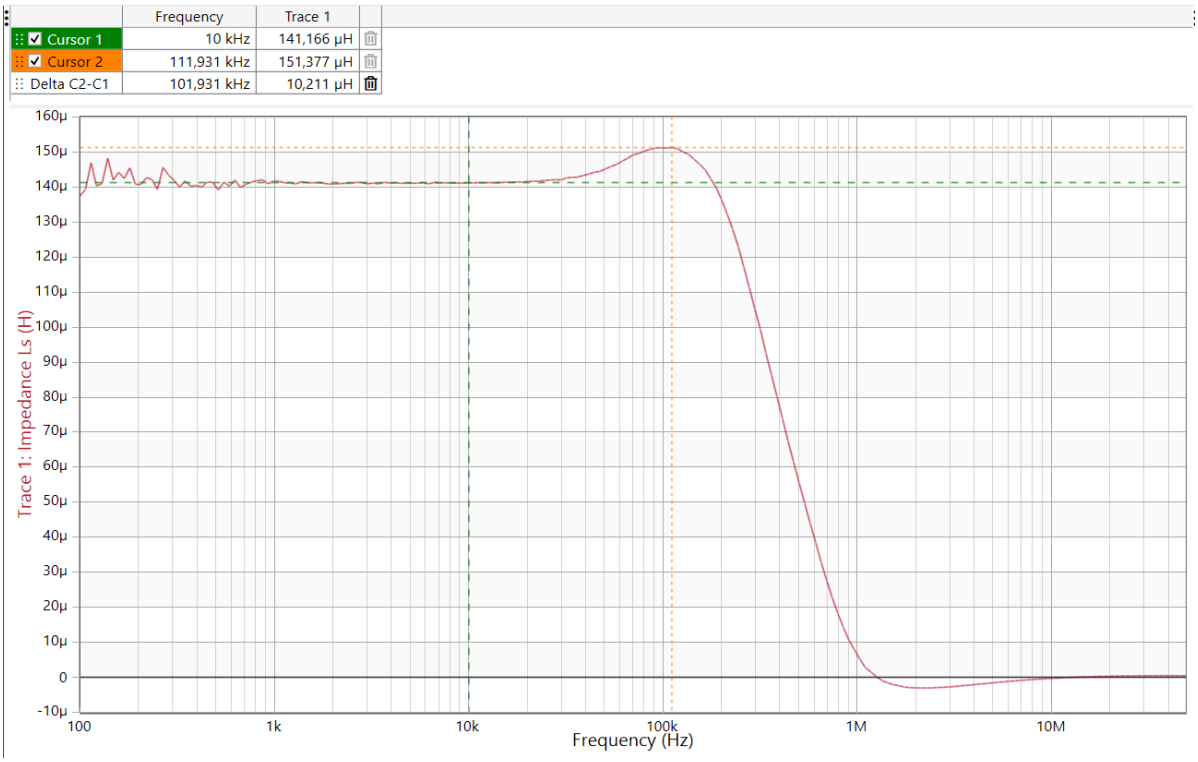

Figure C.7: Inductance plot of Medium Toroid with 5 turns in configuration 2

C.8. Large Toroid 5 Turns Primary Inductance, Config. 1

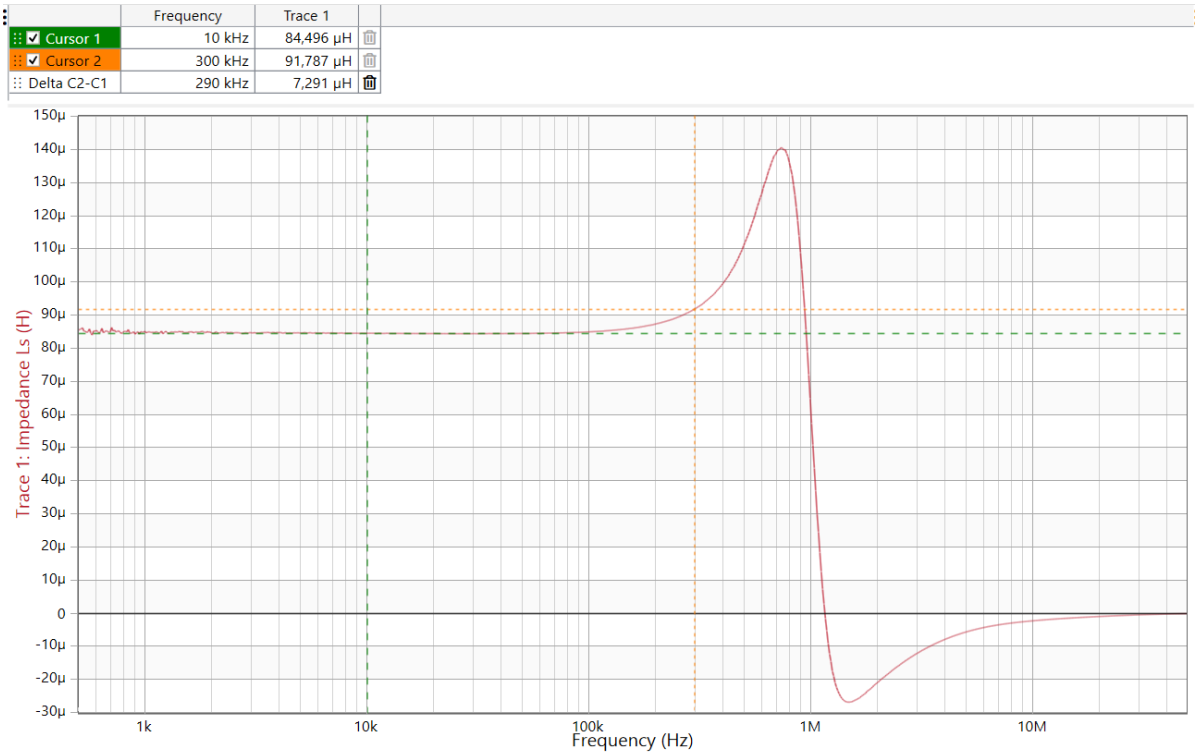

Figure C.8: Inductance plot of Large Toroid with 5 turns

C.9. Large Toroid 20 Turns Primary Inductance, Config. 1

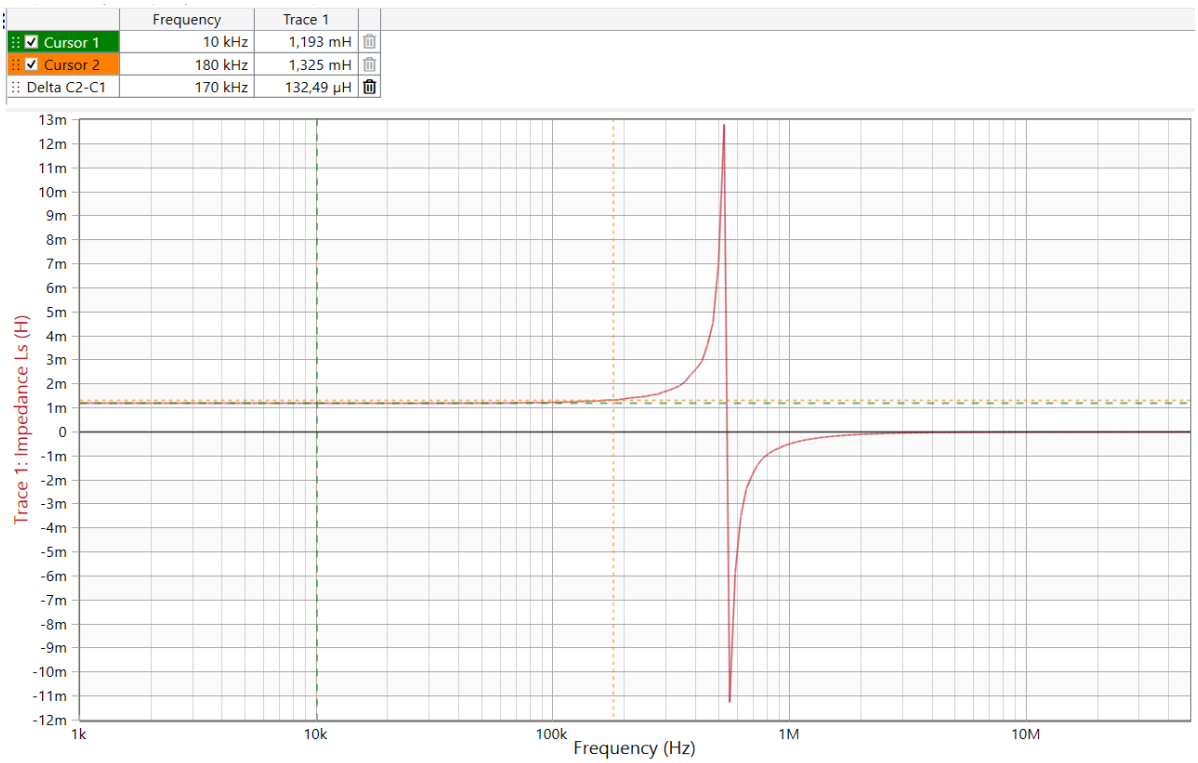

Figure C.9: Inductance plot of Large Toroid with 20 turns

C.10. Large Toroid 13 Turns Primary Inductance, Config. 2

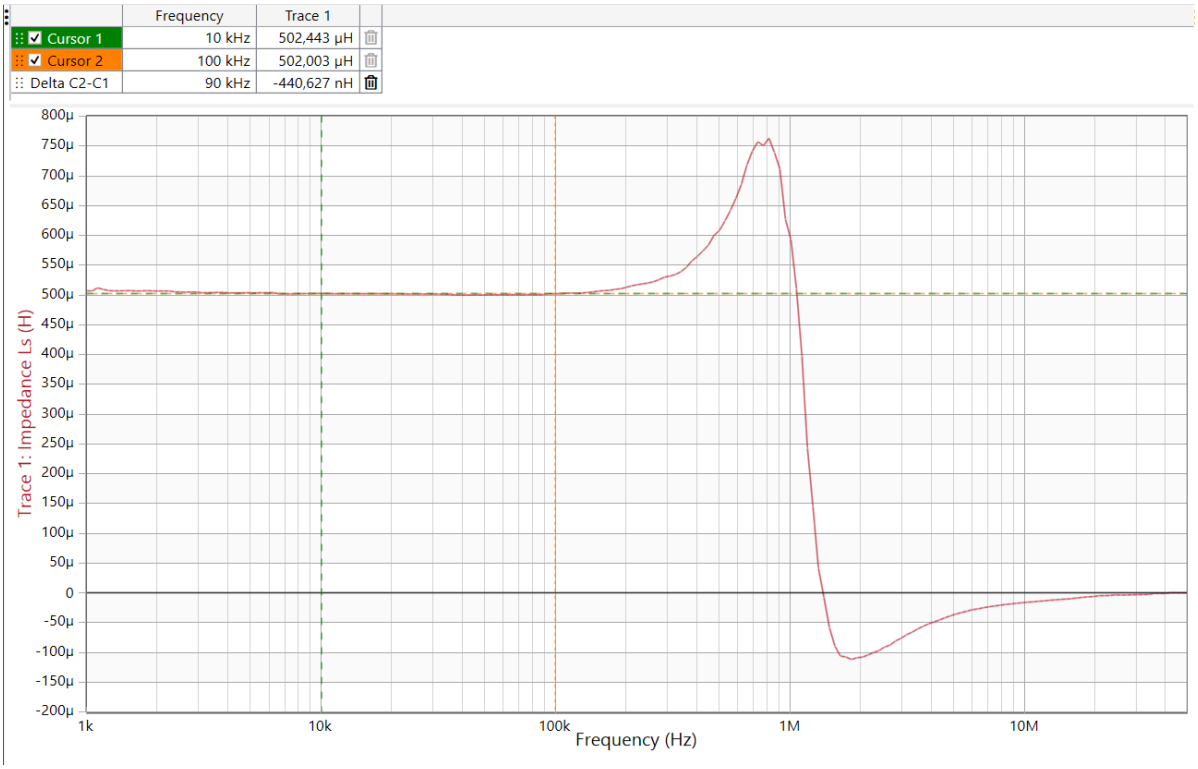

Figure C.10: Inductance plot of Large Toroid with 13 turns in configuration 2

D

Oscilloscope Saturation Graphs

D.1. Tiny 1 Turn

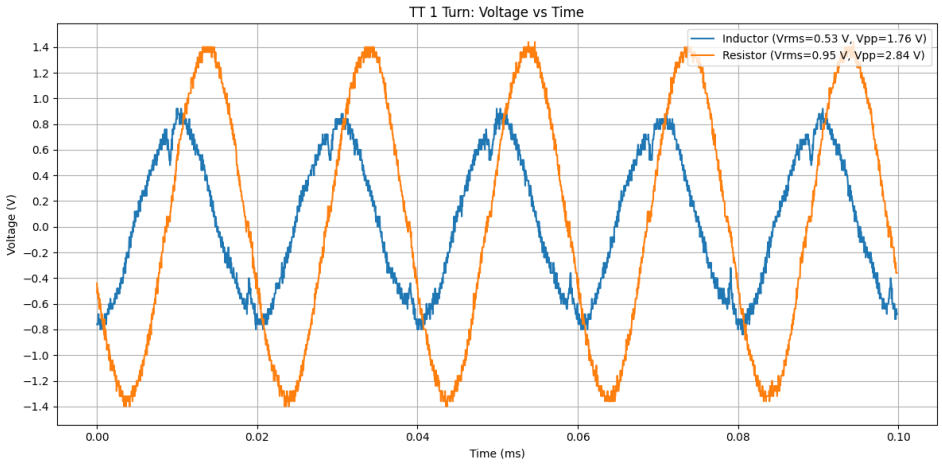

Figure D.1: Tiny Toroid with 1 turn, pre-saturation

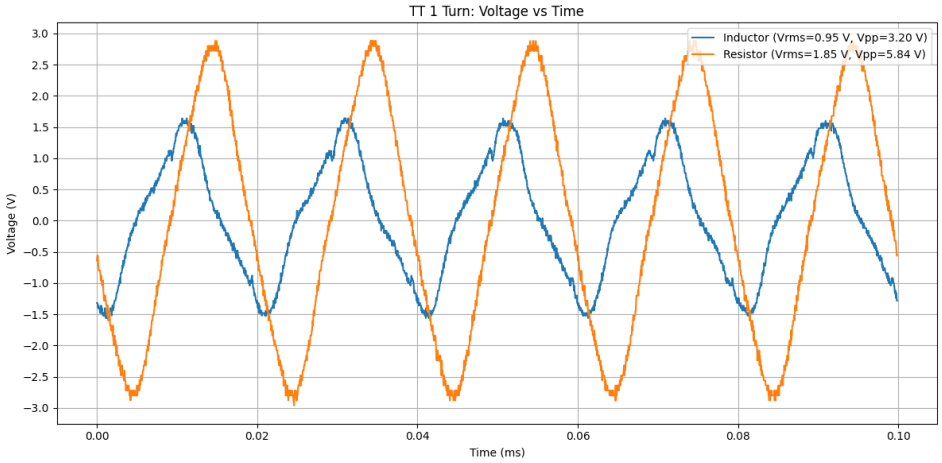

Figure D.2: Tiny Toroid with 1 turn, saturation

D.2. Tiny 3 Turns

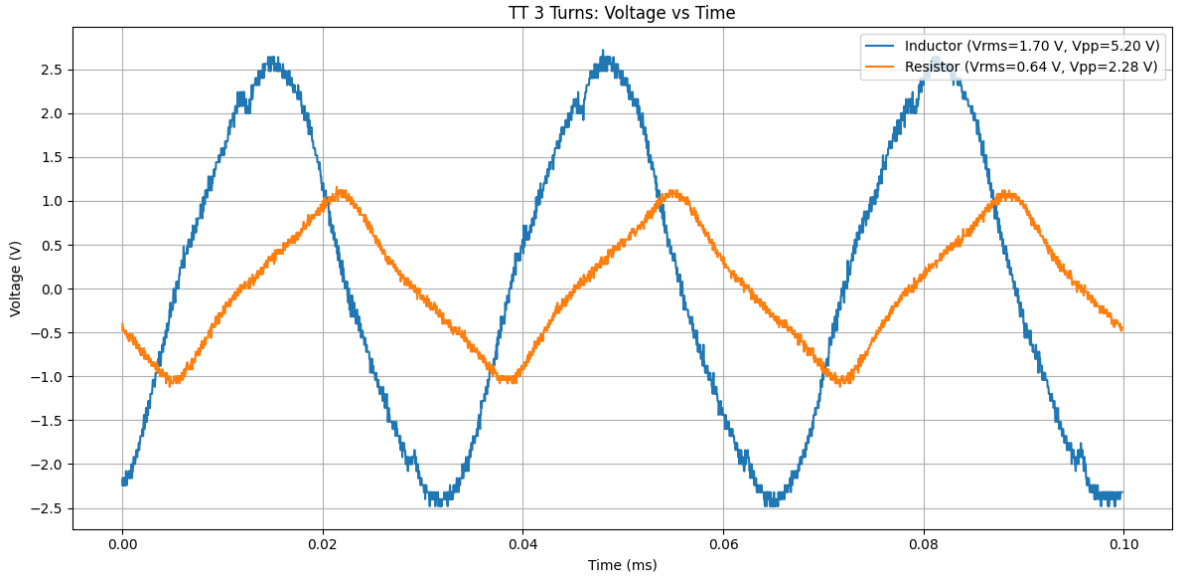

Figure D.3: Tiny Toroid with 3 turns, pre-saturation

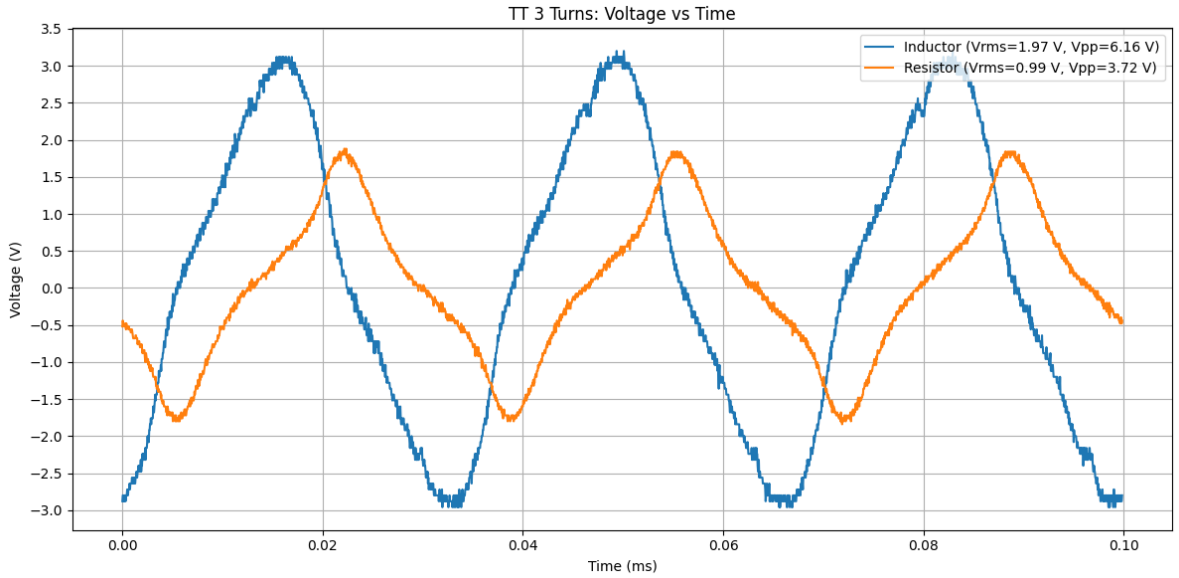

Figure D.4: Tiny Toroid with 3 turns, saturation

D.3. Medium 5 Turns

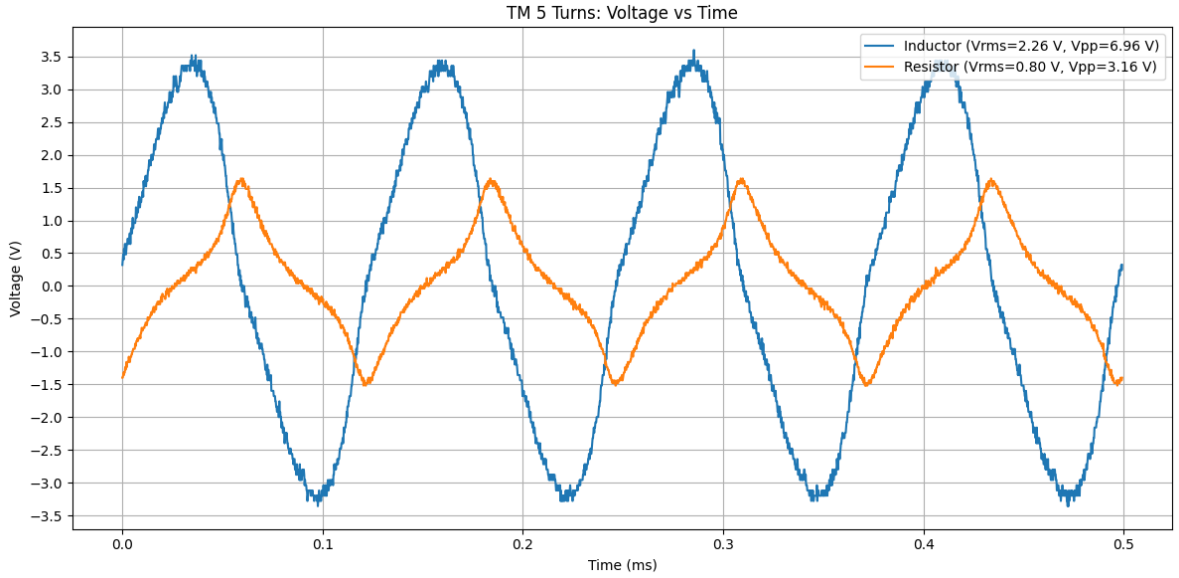

Figure D.5: Medium Toroid with 5 turns, right after saturation

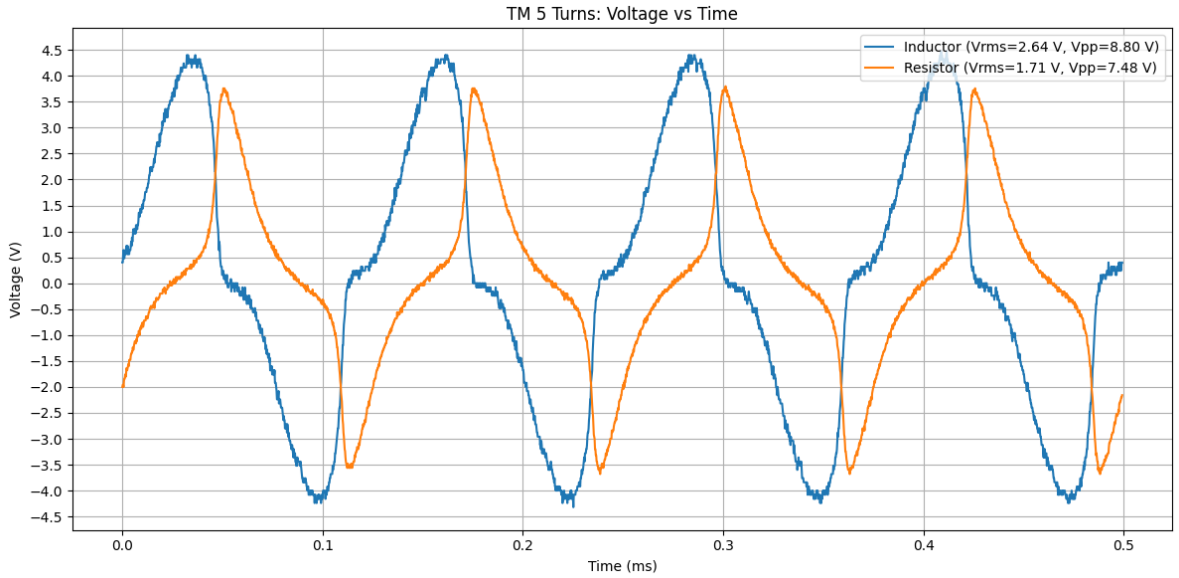

Figure D.6: Medium Toroid with 5 turns, saturation

D.4. Large 5 Turns

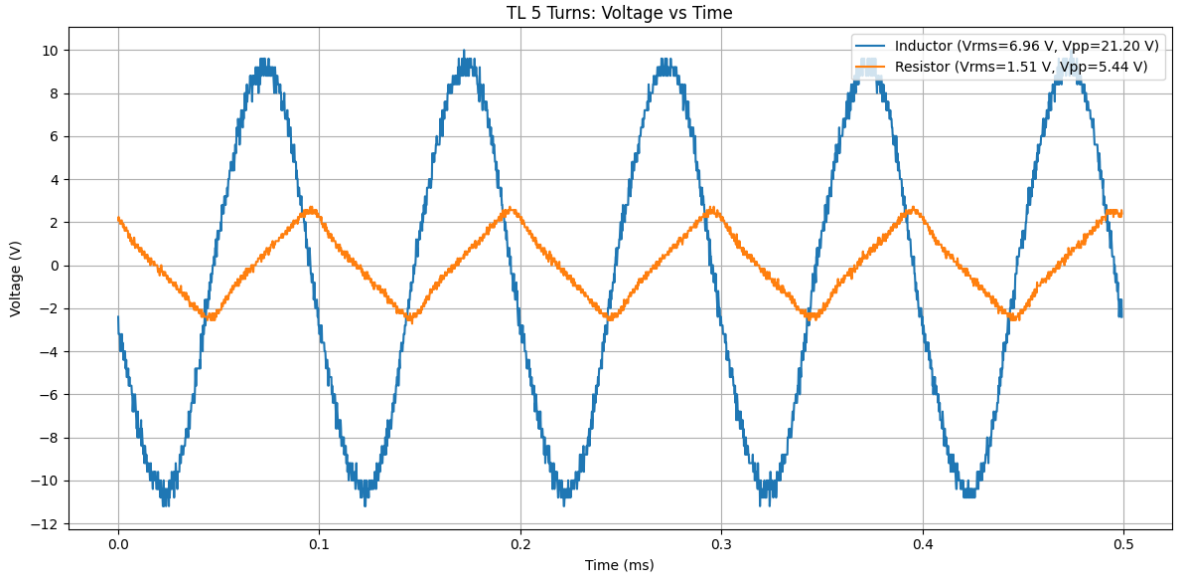

Figure D.7: Large Toroid with 5 turns, pre-saturation

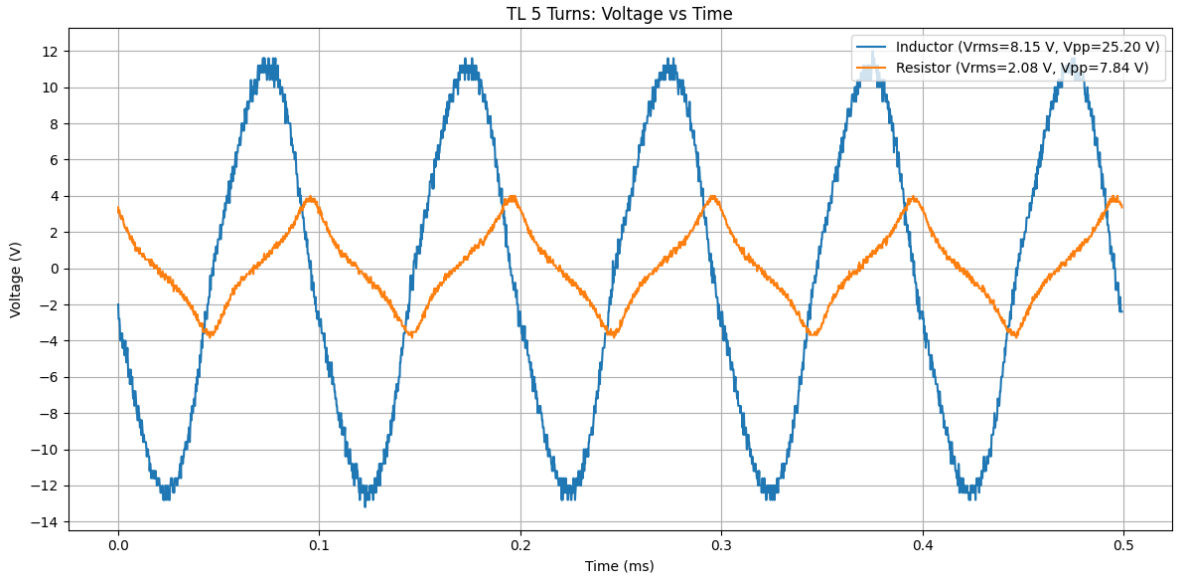

Figure D.8: Large Toroid with 5 turns, saturation

D.5. Large 20 Turns

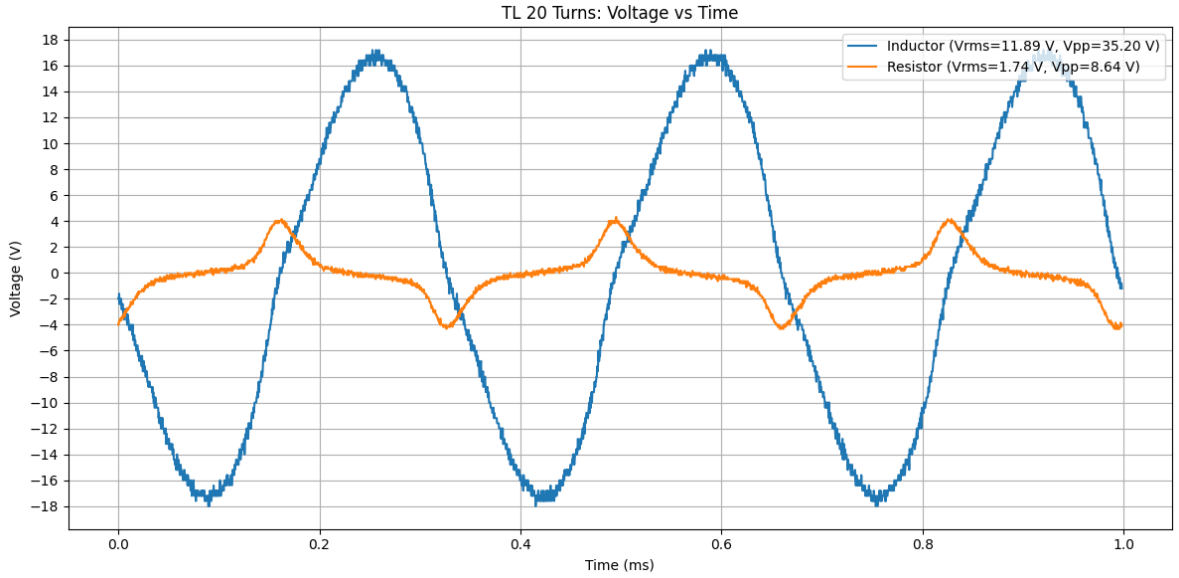

Figure D.9: Large Toroid with 20 turns, saturation

E

Excel sheet

E.1. Data Collection Sheets

	configuration 1					opp ends
Core size	tiny	mid	mid	mid (length of large config 1)	large	large
Turns	3 turn	5 turns	5 turns new	10 turn	5 turns	20 turns
Freq L1 Measured	2.00E+04	1.00E+04	10000	2000	1.00E+05	2.00E+03
R_DC_prim	4.30E-03	6.45E-03		1.15E-02	1.15E-02	3.74E-02
R_DC_sec	4.58E-03	6.89E-03		1.13E-02	1.13E-02	3.84E-02
chosen freq	2.00E+04	1.00E+04	1.00E+04	2.00E+03	1.00E+05	2.00E+03
L1=L_l1+L_mag1	1.90E-05	1.59E-04	9.28E-05	6.43E-04	8.45E-05	1.33E-03
L1 Shorted	8.56E-07	2.53E-06	2.53E-06	8.28E-06	3.80E-06	3.76E-05
k (coupling factor)	0.9772427352716	0.9919906254630	0.9862683287263	0.9935421805207	0.9772308414095	0.9857028485201
L_mag1	1.86E-05	1.57E-04	9.16E-05	6.39E-04	8.26E-05	1.31E-03
L_l1	4.33E-07	1.27E-06	1.27E-06	4.15E-06	1.92E-06	1.90E-05
L2	2.08E-05	1.58E-04	9.28E-05	6.42E-04	8.39E-05	1.31E-03
L_mag2	1.86E-05	1.57E-04	9.16E-05	6.39E-04	8.26E-05	1.31E-03
L_l2	2.24E-06	6.67E-07	1.27E-06	2.38E-06	1.34E-06	2.95E-06
Interwinding C_12	1.00E-15	3.13E-12		1.58E-11	5.18E-12	1.57E-11
L_c1	2.43E-06	1.94E-06	2.53E-06	6.52E-06	3.24E-06	2.19E-05
C_c1	1.33E-11	6.60E-11	#DIV/0!	6.20E-11	7.20E-12	1.04E-10
C_1	1.33E-11	6.29E-11	#DIV/0!	4.62E-11	2.02E-12	8.81E-11
				924.0667333		
L_c2	2.67E-06	1.93E-06	2.53E-06	6.50E-06	3.22E-06	2.16E-05
C_2 calc	1.52E-11	6.31E-11	#DIV/0!	4.63E-11	4.25E-13	8.94E-11
res freq C2	2.50E+07	1.41E+07		7.92E+06	3.75E+07	3.34E+06
res freq C1	2.80E+07	1.41E+07		7.92E+06	3.30E+07	3.34E+06

Figure E.1: Found values for transformers in configuration 1.

				configuration 3		intertwined
Core size	medium litz wire	medium litz wire	large	tiny	mid	large
Turns	thick 5 turns	thin 5 turns		3 turns	5 turns	13 turns
Freq L1 Measured	10000	10000		10000	1.00E+04	1.00E+04
R_DC_prim	1.21E-03	3.85E-03		0.00411	6.21E-03	2.42E-02
R_DC_sec	1.25E-03	3.55E-03		0.0042	5.47E-03	2.41E-02
chosen freq	1.00E+04	1.00E+04		1.00E+04	1.00E+04	1.00E+04
L1=L_l1+L_mag1	1.53E-04	1.53E-04		2.08E-05	9.14E-05	5.02E-04
L1 Shorted	2.01E-06	2.34E-06		4.09E-07	5.11E-07	0.0000003877470
k (coupling factor)	0.9934026409214	0.9923087785594	#DIV/0!	0.9901508447295	0.9971990700180	0.9996140638468
L_mag1	1.52E-04	1.52E-04	#DIV/0!	2.06E-05	9.11E-05	5.02E-04
L_l1	1.01E-06	1.18E-06	#DIV/0!	2.05E-07	2.56E-07	1.94E-07
L2	1.53E-04	1.52E-04		2.07E-05	9.15E-05	4.94E-04
L_mag2	1.52E-04	1.52E-04	#DIV/0!	2.06E-05	9.11E-05	4.89E-04
L_l2	1.01E-06	5.55E-07	#DIV/0!	5.92E-08	4.38E-07	5.00E-06
Interwinding C_12		5.63E-12	4.5pf	6.00E-12	1.10E-11	4.30E-11
L_c1	2.01E-06	1.73E-06	#DIV/0!	2.64E-07	6.92E-07	5.14E-06
C_c1	#DIV/0!	6.23E-11	#DIV/0!	3.84E-11	1.47E-11	3.56E-09
C_1	#DIV/0!	5.67E-11	#DIV/0!	3.24E-11	3.68E-12	3.51E-09
L_c2	2.01E-06	1.72E-06	#DIV/0!	2.62E-07	6.93E-07	5.19E-06
C_2 calc	#DIV/0!	#DIV/0!	#DIV/0!	3.26E-11	3.65E-12	3.67E-09
res freq C2				5.00E+07	5.00E+07	1.15E+06
res freq C1		1.53E+07		5.00E+07	5.00E+07	1.18E+06

Figure E.2: Found values for transformers in configuration 2&3.

E.2. Number of Turns Sheets

	Reluctance	4.35E+05	1.64E+05	3.18E+05
Desired Leakage	L1 / Lmag	tiny N	mid N	big N
1.29E-06	8.79E-05	6.187976293	3.798483205	5.291867414
2.58E-06	1.76E-04	8.751119997	5.371866465	7.483830667
average (1-k)	Average	7.469548145	4.585174835	6.38784904
0.0146704066815	100k	tiny 6 turn	mid 5 turn	
	Ls	7.70E-05	1.62E-04	
	gain	0.987896	0.983154	
	omega	628318.5307	628318.5307	
	Lmag1	7.61E-05	1.59E-04	
	Ll1	9.32E-07	2.72E-06	
	resistance R1	6.70E-03	8.00E-03	
	1.5% L1	1.16E-06	2.43E-06	
	k	0.9875474508	0.9940910251	

Figure E.3: Desired leakage for prototyping

	config 1							
wire resistances	tiny 1 turn	tiny 2 turn	tiny 3 turn	tiny braided 3	mid 5	mid 10	large 5	large 20
turns	1	2	3	3	5	10	5	20
core circumference mm	17.25	17.25	17.25	17.25	28.50	28.50	47.10	47.10
tot wire length + 3 cm on	0.07725	0.0945	0.11175	0.11175	0.2025	0.345	0.2955	1.002
calc using core dimensio	3.01E-03	3.69E-03	4.36E-03	4.36E-03	7.90E-03	1.35E-02	1.15E-02	3.91E-02
percentage difference	-28.22	-12.20	1.42	5.85	22.52	17.17	0.36	4.58
measured	4.20E-03	4.20E-03	4.30E-03	4.12E-03	6.45E-03	1.15E-02	1.15E-02	3.74E-02

Figure E.4: Winding resistance calculations.

Capacitance calculation block (BIG 20 N)		Capacitance calculation block(BIG 5 N)			
Eps_0	8.85E-12	Eps_0	8.85E-12		
Area	5.08E-04	Area	9.09E-05		
distance_between wires	1.85E-02	distance_between wires	2.06E-02		
length	2.00E-02	length	3.75E-03		
width	0.0174	width	1.70E-02		
width+fringe error	0.0254	width+fringe error	2.43E-02		
C12_meas	1.57E-11	C12_meas	4.59E-12		
C12_calc	2.43E-13	C12_calc	3.92E-14		

Capacitance calculation block (Tiny 3 N)		Capacitance calculation block(Mid 5 N)		Capacitance calculation block(MID 10 N)	
Eps_0	8.85E-12	Eps_0	8.85E-12	Eps_0	8.85E-12
Area	6.75E-06	Area	6.83E-05	Area	1.30E-04
distance_between wires	6.90E-03	distance_between wires	1.67E-02	distance_between wires	1.62E-02
length	7.50E-04	length	3.75E-03	length	7.13E-03
width	5.75E-03	width	9.00E-03	width	0.009
width+fringe error	9.00E-03	width+fringe error	1.82E-02	width+fringe error	1.82E-02
C12_meas	1.57E-11	C12_meas	4.59E-12	C12_meas	4.59E-12
C12_calc	8.66E-15	C12_calc	3.63E-14	C12_calc	7.08E-14

Figure E.5: Interwinding capacitance calculations

x	tiny 1 turn, config 1	tiny 2 turn	tiny 3 turn	tiny braided	tiny 3 turn config 2	mid 5, config 1	mid 10	mid 5, config 2	large, 5 config 1	large 20	large 13 config 2
Material	Tiny->3E65					Medium->3E10-M			Large->3C94	3C94	3C94
initial permeability	5200	5200	5200	5200	5200	10000	10000	10000	2300	2300	2300
perm @ 100C	0	0	0	0	0	0	0	0	5500	5500	5500
mew_0	1.26E-06	1.26E-06	1.26E-06	1.26E-06	1.26E-06	1.26E-06	1.26E-06	1.26E-06	1.26E-06	1.26E-06	1.26E-06
Ae_core	1.23E-05	1.23E-05	1.23E-05	1.23E-05	1.23E-05	3.55E-05	3.55E-05	3.55E-05	9.75E-05	9.75E-05	9.75E-05
path length	3.50E-02	3.50E-02	3.50E-02	3.50E-02	3.50E-02	7.32E-02	7.32E-02	7.32E-02	8.97E-02	8.97E-02	8.97E-02
number of turns prim.	1	2	3	3	3	5	10	5	5	20	13
Reluctance init perm	4.35E+05	4.35E+05	4.35E+05	4.35E+05	4.35E+05	1.64E+05	1.64E+05	1.64E+05	3.18E+05	3.18E+05	3.18E+05
Reluctance perm @ 100C	#DIV/0!								1.33E+05	1.33E+05	1.33E+05
L init perm	2.30E-06	9.19E-06	2.07E-05	2.07E-05	2.07E-05	1.52E-04	6.09E-04	1.52E-04	7.85E-05	1.26E-03	5.31E-04
L perm @ 100C	#DIV/0!								1.88E-04	3.00E-03	1.27E-03
Imag 1 measured	2.44E-06	8.74E-06	1.86E-05	1.95E-05	2.06E-05	1.57E-04	6.39E-04	9.11E-05	8.26E-05	1.31E-03	5.02E-04
L1 measured	2.78E-06	9.13E-06	1.90E-05	1.98E-05	2.08E-05	1.59E-04	6.43E-04	9.14E-05	8.45E-05	1.33E-03	5.02E-04
percent deviation	20.93	-0.61	-7.94	-4.35	0.87	4.20	5.57	-40.04	7.64	5.57	-5.32
leakage (1-k)L_calc=Ll1	2.30E-06	3.99E-07	4.70E-07	3.13E-07	2.04E-07	1.22E-06	3.94E-06	4.27E-07	1.79E-06	1.80E-05	2.05E-07

Figure E.6: Magnetising inductance calculations

	A	B	C	D
1	Frequency (kHz)	Toroid tiny (12.3, 320mT @ 100C)	toroid medium (35.5, 270mT @ 100C)	toroid large(r) (97.5, 380mT @ 100C)
2	10	202.28	83.06	21.49
3	50	40.46	16.61	4.3
4	100	20.23	8.31	2.15
5	200	10.11	4.15	1.07
6	300	6.74	2.77	0.72
7	400	5.06	2.08	0.54
8	500	4.05	1.66	0.43
9	600	3.37	1.38	0.36
10	700	2.89	1.19	0.31
11	800	2.53	1.04	0.27
12	900	2.25	0.92	0.24
13	1000	2.02	0.83	0.21
14	1200	1.69	0.69	0.18
15	1400	1.44	0.59	0.15
16	1600	1.26	0.52	0.13
17	1800	1.12	0.46	0.12
18	2000	1.01	0.42	0.11
19	3000	0.67	0.28	0.07

Figure E.7: Minimum number of turns required at different frequencies for different cores